Discrete Particle Numerical Simulation of Granular Material Behavior

by Marijan Babić

Report No. 88-11
December, 1988
Department of Civil and Environmental Engineering
Clarkson University
Potsdam, New York 13676

Abstract

In this report, a numerical model for dynamical simulation of granular material behavior is described. The idealized granular material consisting of uniform circular disks is considered. The model calculates the motion of individual particles as they interact with each other and boundaries. The soft-particle approach is used, which allows for non-instantaneous and simultaneous contacts between particles. The contact force model is viscoelastic with friction limit on tangential force component. This approach is applicable to both quasi-static and dynamic problems.

The preliminary results of the model are reported. These results include the nine-disc verification test, two illustrative examples of general flows, the slow deformation of material in rectangular wall bounded system and profiles of concentration and velocity in uniform rectilinear flows (wall-driven Couette flow and gravity-driven channel flow).

The model is intended to be used to provide guidance for theoretical efforts to derive general constitutive equations for granular flow, including quasi-static, transitional and rapid flow regimes. In addition, the model is capable of performing numerical experiment (direct simulation) of any two-dimensional configuration.

The particular application of such a theory and/or numerical experiment is the problem of ice jams and drift of packed ice in rivers. The closure of the equations governing the motion of ice pans on the water surface requires constitutive expressions for internal stresses, diffusion and dissipation of mechanical energy in variety of regimes (dilute, intermediate, dense, jam). General theory for granular flows should be able to provide these constitutive expressions. In addition, the numerical experiments resembling the process can be devised. For instance, the flow of particles which are subjected to different forcing mechanisms down an inclined channel can be simulated, and possible downstream restrictions on the channel (curvature, contraction, obstacles) can be imposed as well. Having this tool at hand, the ice jam problem can be attacked from different sides to provide better understanding of the complex phenomena involved.

Acknowledgement

The support, encouragement and assistance of Drs. Hayley H. Shen and Hung Tao Shen are very much appreciated.

This study is supported by the U. S. Army Cold regions Research and Engineering Laboratory through Contract No. DACA89-87-K-0001.

Contents

Chapter 1

Introduction

The mechanical behavior of granular solids is important geophysical and industrial problem. Flow of granular material occurs in many technological processes such as pneumatic transport, slurry pipelines, powder processing, material handling in bins and hoppers, as well as in many geophysical phenomena such as sediment transport in rivers, ice jams acn drift of packed ice, landslides, snow avalanches, rock falls, debris flows etc.

In search for the constitutive equations describing the behavior of granular material in a variety of regimes such as grain-inertia (rapid flow), quasi-static (slow flow), macroviscous (suspended particles), transitional etc., current research efforts include theoretical, experimental and numerical models.

Discrete particle numerical simulations of granular material motion have become a valuable tool for investigation of behavior of particulate media. These models determine the behavior of an idealized granular material by calculating the motion of individual particles as they interact with each other and the boundaries. The macroscopic properties are then determined by appropriate space and time averaging.

This approach originates from ideas and methods of molecular dynamics, which began in 1950's and has undergone extensive development since then. The success of molecular dynamics calculations in predicting equilibrium equations of state and nonequilibrium transport properties has been one of major motivating factors for adaptation of these techniques to granular materials.

There are two basic techniques used for numerical simulation of behavior of system of particles. These are rigid-particle and soft-particle models. These methods are compared and principal existing models are reviewed in Table 1.1.

1.1 Rigid Particle Models

In rigid-particle models collisions are assumed to be instantaneous. Post-collision trajectories are determined from the initial trajectories and inelastic, frictional collisional operator governing the dynamics of idealized binary collision. The "predictor" search strategy is used. The list of collisions in order of precedence is maintained and simulation proceeds by variable time steps between successive collisions. Such models are particularly well suited for dynamic situations with significant granular temperature (vibrational kinetic energy). In high density situations time between collisions becomes very small, so that in the limit of continuous and/or simultaneous contacts this approach can not be efficiently used.

The rigid-particle model for granular flow was developed by Campbell (1982). He modeled rectilinear uniform shear flows using streamwise periodic boundaries. Campbell and Brennen (1985a, 1985b) reported results of shear (Couette) flow and chute flow simulation. Campbell and Gong (1986) performed a detailed study of the stress tensor in a simple shear flow using both transverse and streamwise periodic boundaries. They used a collision operator that produces zero relative tangential post-collisional velocities corresponding to an infinite coefficient of friction.

Hopkins (1985) and Hopkins and Shen (1986) have developed Monte Carlo simulation of simple shear flow. A large ensemble of particles is created which represents statistically meaningful sample of the particles in the flow. Two particles are selected at random. One of the selected particles is placed at the origin and the other is assigned a random pre-collision position such that the distance it has to travel before collision equals the expected mean free path for a system at modeled concentration. The difference between fluctuation velocities, which are stored for all particles, is then added to the relative position dependent mean field velocity to determine the total relative precollisional velocity. A rigid-body inelastic, frictional operator is then applied to determine post-collisional velocities. The post-collision fluctuation velocities are then assigned to these two particles and they are put back into the statistical ensemble. The process is repeated several thousand times until a steady state velocity distribution is established in the ensemble. The stress tensor and other various statistics are obtained by averaging over all executed collisions. The drawback of the method is that concentration dependent variables such as the mean free path have to be prescribed a priori, usually from established results of kinetic theory of gases.

Hopkins (1987) has developed dynamical rigid-particle numerical simulation similar to Campbell's with motivation to provide the spatial context for the Monte Carlo simulation as well as to provide a check for two-dimensional air-table experiments of Sanders and Ackermann (1987). In his simulation the collisional operator is used which is capable of explicitly accounting for finite values of friction coefficient. A "hybrid" search strategy is devised which does not require complicated maintenance of collision list but rather allows for the small overlap between particles. These overlaps are searched for only in immediate neighbourhood of each particle. Hopkins (1987) has applied this dynamical simulation to the simple shear flow and wall-bounded Couette and gravity driven flows.

1.2 Soft Particle Models

The soft particle approach requires that collisions are of finite durations. The duration of contact is related to non-infinite particle stiffness which is specified as particle property. The force at the contact is continuously varying as the particles are being deformed. Deformation of the particle is represented as the small overlap. Various contact force models can be incorporated (elastic, viscoelastic, Hertzian etc.). Forces at all contacts are determined at one instant and Newton's equations of motion are then numerically integrated to obtain new particle positions and velocities. Simulation proceeds by small time step which is usually kept at a fixed value. In order to accurately integrate equations of motion the usual explicit schemes require more than 10 time steps during a collision. This approach is not very efficient for dilute systems with only occasional collisions. However, for dense systems this approach is much more efficient than a rigid particle approach. More importantly, this approach can be applied to all configurations, including static and dynamic situations.

Cundall and Strack (1979a, 1979b, 1982, 1983) developed the first discrete particle model based on the soft particle approach. They used viscoelastic normal force model (damped harmonic oscillator), consisting of the linear spring and velocity proportional dashpot terms. Shear force is viscoelastic below the Mohr-Coulomb friction limit, and purely frictional at the friction limit, corresponding to the sliding at the contact. In addition to friction damping which occurs during sliding, energy is dissipated through two forms of damping: contact damping corresponding to inelastic contacts, and global damping which operates on absolute velocities of the disks and is introduced in calculation of motion. The main calculation cycle is divided into two parts. In the first part, all current contacts are detected and the forces at every contact are calculated from current positions and velocities based on the assumed force-displacement law. The contact forces are resolved into components in global coordinate directions and summed, for each particle. The second part of calculation cycle takes these forces and moments and integrates equations of motion to obtain new velocities and positions. The time is incremented one time step and the cycle is repeated. The whole cycle described above is repeated many thousands of times during a typical run.

Although their calculation method treats the full dynamics of system of particles, it was used primarily to investigate the behavior of granular material undergoing slow, quasi-static deformations. They applied such a loading rates on the material so that inertial forces remain much smaller than typical contact forces. They have demonstrated that stress networks exist in granular solids under external loading. Load is supported primarily by several stess bearing columns alligned in direction of largest principal stress. These columns fail during deformation by buckling, but are created again nearby. Sliding and frictional energy losses occur mostly in the lightly loaded regions near the buckling stress columns. Thay have also provided informations on the contact angle distributions, contact force distributions and other various statistics of interest. Simulated stress-strain curves are in good qualitative agreement with experimental measurements.

Several models are patterned after programs of Cundall and Strack, and various adaptations and extensions are used for further studies. Thornton (1985) has examined stresses in simulated materials under quasi-static deformations through various stress-strain histories. Haff and Werner (1986) have examined the problem of mechanical sorting of particles using similar model. Haff (1987) studied the transmission of sound waves through granular material.

Walton (1982,1983) has developed an explicit particle-dynamics model for granular materials, similar to model of Cundall and Strack. The difference in force model is only the inclusion of the damping or dashpot normal force in determining the total normal force used for the friction limit, what is more suitable for rapid particle

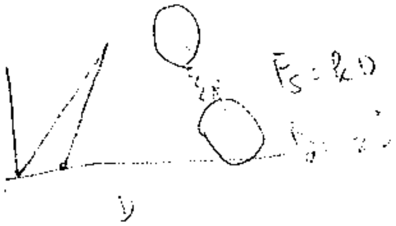

interactions with dynamic impacts. This model is intended to be used for rapidly deforming granular material. There are two versions of this model, one which calculates the motion of two-dimensional polygonal particles, and the other uses circular discs. Model was applied to bin and chute flows as well as direct shear of oil shale rubble.

Walton and Braun (1985, 1986) use a different force model in their study of assemblies of nearly rigid, inelastic, frictional disks undergoing steady-state shearing. The normal force model is partially latching spring model. Force-displacement law has different slopes for loading and unloading portions of an impact. Thus, the normal force exibits a position dependent hysteresis which results in a less than unity coefficient of restitution for normal impacts. The tangential friction force model is patterned after theoretical models for the friction forces acting between elastic spheres in contact developed by Mindlin and Deresiewitz (1953).

The periodic boundaries in all directions are used to simulate simple shear flow. At the steady state condition energy introduced into the system by uniform shearing is dissipated through inelastic normal forces and through frictional sliding. Resulting kinetic energy density (granular temperature), viscosity, pressure and stresses are all functions of the applied strain rate, concentration and material properties. The comprehensive parameter study is performed for the simple shear flows of disks (Walton and Braun (1985)) and spheres (Walton and Braun (1986)).

In this report, a numerical model DINAMO and its preliminary results are described. The motivation for development of this model is to provide guidance for theoretical efforts to derive the constitutive equations for quasi-static and transitional regimes and unify these with kinetic theory for rapid flow regime. In this sense, the numerical results will provide detailed informations on general material behavior as well as specific informations on various statistical distributions. In addition, the model is capable of direct simulation of any two-dimensional configuration and can be used for verification of theoretical and experimental results.

<table>
<tr><td>approach</td><td colspan="2">Soft-particle</td><td colspan="2">Rigid-particle</td></tr>
<tr><td>contacts</td><td colspan="2">finite-duration (multiple)</td><td colspan="2">instantaneous (binary)</td></tr>
<tr><td>strategy</td><td colspan="2">detector (overlap)</td><td colspan="2">predictor (collision list)</td></tr>
<tr><td>applies to</td><td colspan="2">static and dynamic</td><td colspan="2">rapid flow</td></tr>
<tr><td>suited for</td><td colspan="2">moderate to high densities</td><td colspan="2">significant gran. temp.</td></tr>
<tr><td>limitations</td><td colspan="2">low densities</td><td colspan="2">high densities</td></tr>
<tr><td>researchers</td><td>Cundall</td><td>Walton</td><td>Campbell</td><td>Hopkins</td></tr>
<tr><td>year</td><td>1971-</td><td>1985-</td><td>1982-</td><td>1987</td></tr>
<tr><td>contact model (normal dir.)</td><td>harmonic oscillator</td><td>partially latching spring</td><td>rigid-body collision</td><td>rigid-body collision</td></tr>
<tr><td>contact model (shear dir.)</td><td>friction-constrained</td><td>incrementally slipping</td><td>infinite friction</td><td>finite friction</td></tr>
<tr><td>problems studied</td><td>quasi-static deformations</td><td>rapid flow (simple shear)</td><td>Couette, chute, simple shear</td><td>Couette, simple shear</td></tr>
<tr><td>motivation</td><td>soil & rock mechanics</td><td>gran. flows (fundamental)</td><td>industrial, fundamental</td><td>air-table, Monte Carlo</td></tr>
<tr><td>adaptations; extensions</td><td>Walton (1982), Thornton, Haff, others</td><td></td><td></td><td></td></tr>
</table>

Table 1.1: Review of existing numerical models

Chapter 2

Numerical Model

In this chapter the main features of the present numerical model are described.

The model is capable of simulating various system configurations, described in section 2.1. Presently, these configurations are:

- general system;
- rectangular wall bounded system (quasi-static problems);
- uniform rectilinear flows (Couette, channel and chute flows).

The program is basically divided in three units:

- input and initialization unit (described in section 2.2);
- the main unit which performs calculation cycle (described in section 2.3);
- statistical description and output unit.

The principal flow chart of the simulation is given in Figure 2.1.

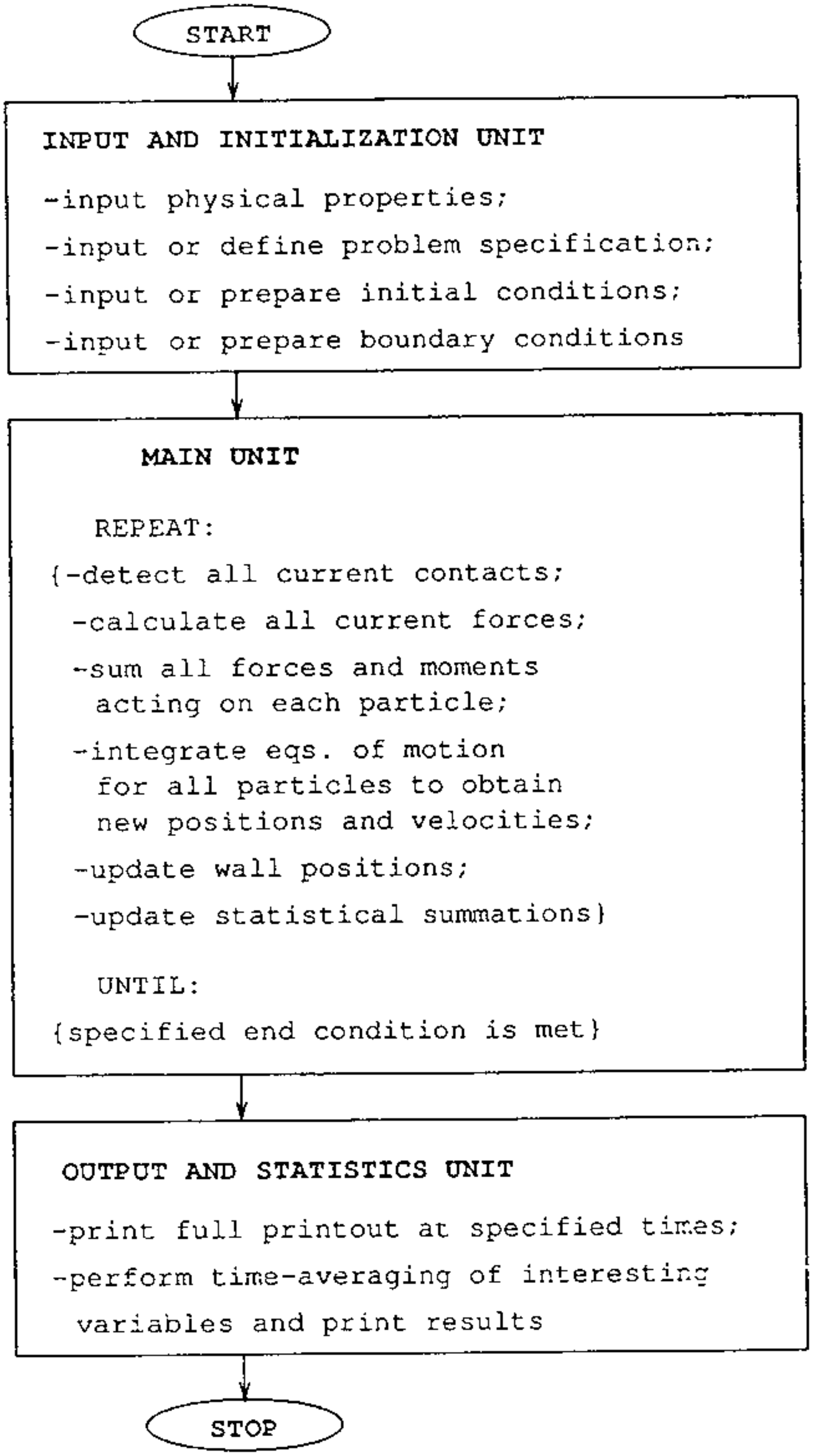

Figure 2.1. Principal Flow Chart

2.1 System Configuration

2.1.1 General System

The basic version of the model can handle any two-dimensional problem including the problems with very complex geometry. However, it is also the simplest version because the initial condition is not automatically generated but is read from an input file instead. Therefore, it is typically used in conjunction with one or more supplementary programs which can prepare desired initial condition (regular, random, etc.). The initial conditions include the initial coordinates and velocities of all particles and walls. The further course of simulation is then determined by user-specified motion of walls and/or action of body forces such as gravity. These "boundary conditions" are currently represented as step-functions, i.e. wall velocities and rotations are assumed to be constant over finite intervals of time (specified number of time steps).

Several example runs (two-dimensional hopper, cascade of chutes, etc.) have been performed in order to demonstrate rather wide capabilities of the model as well as for verification purpose. These results are presented in chapter 3.

2.1.2 Rectangular Wall Bounded System

This version is intended to be used for the quasi-static problems similar to the problems investigated by Cundall and Strack. Initially, particles are contained in rectangular area of dimensions (a,b) bounded by rigid walls. The motion of walls is prescribed as a function of time. The granular material in this "box" is undergoing slow deformation as it is being subjected to external time-dependent loading, caused by the motion of walls. Several problems of interest such as compression test, shear test, biaxial test etc. may be investigated in this manner. Some preliminary results as well as comparison with Cundall and Strack are reported in chapter 3.

2.1.3 Uniform Rectilinear Flow

This version is intended to be used for investigation of steady, uniform rectilinear flows such as Couette flow, channel flow and chute flow. Boundary conditions for uniform rectilinear flows are shown in Figure 2.2.

The streamwise periodic boundary is used to simulate uniform flow with only limited number of particles. The particle which leaves the control area on the downstream side automatically enters the control area at the upstream side. Rigid walls can be either flat or artificially roughened by placing semi-particles on the wall at the specified spacing. These "bumpy" walls are used in air-table experiments of Sanders and Ackermann (1987). In these experiments Couette and channel (gravity) flows were investigated. Hopkins (1987) performed rigid-particle dynamical simulation used for verification of these experiments. Couette and chute flow numerical experiments were also performed by Campbell and Brennen (1985a, 1985b).

Couette flow is shown in Figure 2.3.a. The flow plane is horizontal. The flow is driven by motion of walls with velocity U_o in opposite directions.

Channel flow is shown in Figure 2.3.b. The flow plane is inclined by angle α_o from the horizontal plane. The flow is driven by the component of gravity force acting in the flow direction $g_x = g \sin \alpha_o$. The other component of gravity is perpendicular to the channel plane, and hence does not play any role in the flow.

Both of the above driving mechanisms can be combined as well.

Chute flow configuration is shown in Figure 2.3.c. In this problem the flow plane is the vertical plane. The configurational difference with channel and Couette flow is that only one (bottom) wall is physically present. The inclination angle of this wall is β_o. Flow is driven down the chute by the streamwise component of gravity force $g_x = g \sin \beta_o$, but the transverse component of gravity $g_y = g \cos \beta_o$ is acting on the particles as well.

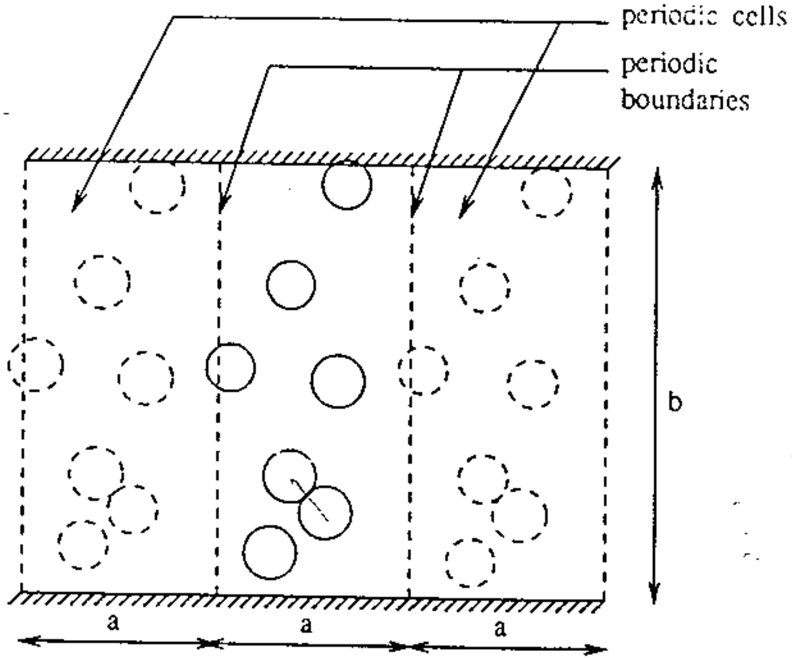

Figure 2.2.a: flat walls

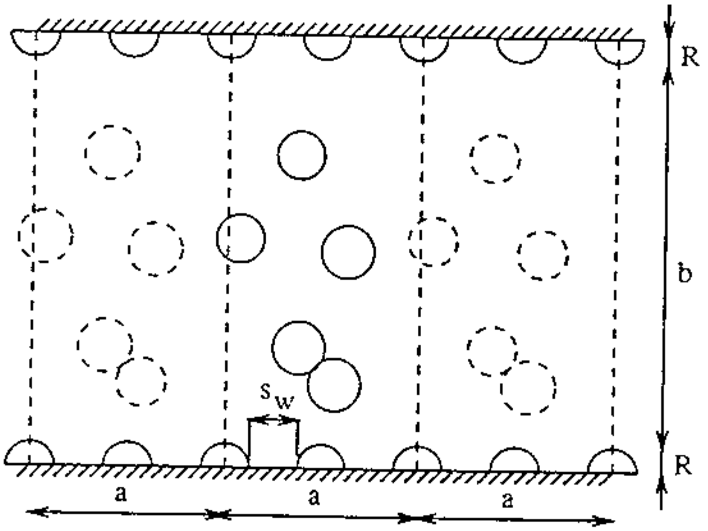

Figure 2.2.b: rough ("bumpy") walls

Figure 2.2. Boundary Conditions for Uniform Rectilinear Flows

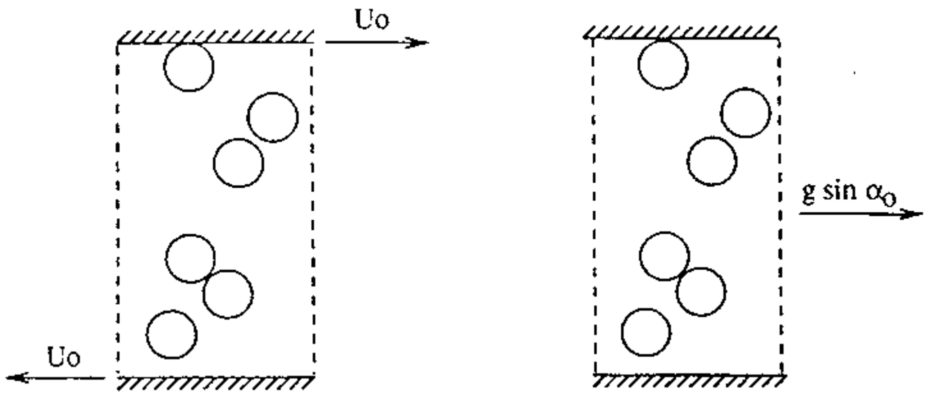

a) Couette flow
(wall driven)

b) channel flow
(gravity driven)

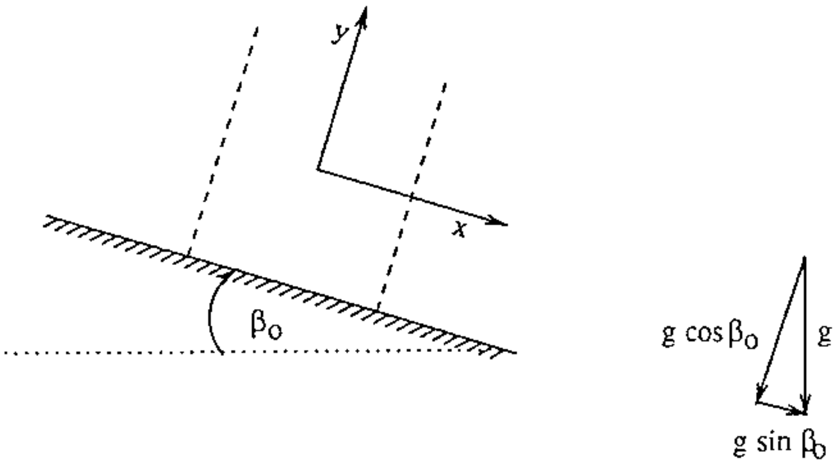

c) chute flow

Figure 2.3. Uniform Rectilinear Flows

2.2 Input and Initialization

The input parameters that must be specified to run numerical simulations with present model can be divided into physical properties data, initial conditions and boundary conditions. In the general version of the model, both initial and boundary conditions are read from input files. The automatic generation of random initial conditions is available for problems with rectangular geometry (rectangular wall bounded system and uniform rectilinear flow).

2.2.1 Physical Properties

An idealized granular material consisting of equal-sized circular particles is considered. The particles are described by the following set of input parameters:

R	radius
th	thickness
ρ_s	density
k_n	normal stiffness
k_s/k_n	shear to normal stiffness ratio
ϵ	coefficient of restitution
ζ_s	dimensionless shear damping coefficient
μ	friction coefficient

The other particle properties used in model are derived from the above input parameters. These are:

$m = \rho_s R^2 \pi$	mass
$I = \frac{1}{2} m R^2$	moment of inertia

$K_n = k_n/2$	effective normal contact stiffness
$K_s = k_s/2$	effective shear contact stiffness
$\zeta_n = \frac{-\ln\epsilon}{\sqrt{\pi^2+\ln^2\epsilon}}$	dimensionless normal damping coefficient
$C_n = 2\zeta_n\sqrt{mK_n}$	normal damping coefficient
$C_s = 2\zeta_s\sqrt{mK_n}$	shear damping coefficient

The coefficients K_n, K_s, ζ_n, ζ_s, C_n, C_s and μ which define the contact force model are explained in section 2.3.4. and in detail in Appendix A.

Time Step

The time step used in the simulation is a function of material (contact) properties. The critical time step (duration of binary collision) was found in Appendix A to be:

$$t_c = \frac{\pi}{\sqrt{\frac{k_n}{m}(1-\zeta_n^2)}} \tag{2.1}$$

The actual time step Δt used in simulation is a fraction (specified by user) of critical time step t_c. This fraction is usually selected to be $\frac{1}{10}$.

$m\ddot{x} + d\dot{y} + kx = 0$

2.2.2 Initial and Boundary Conditions

The initial conditions for the problem include the initial coordinates and velocities of all particles and walls as well as contact forces at all contacts (if any). The boundary conditions for the problem include the velocities and rotations of all walls prescribed as step-functions of time.

In the general version of the model, the initial conditions are read from input file 'DIN.ICS', and the boundary conditions are read from input file 'DIN.BCS'.

Particle Definition

Each particle is described by the following set of informations (Figure 2.4):

P	number of particle
x_P	x-coordinate
y_P	y-coordinate
u_P	velocity in x-direction
v_P	velocity in y-direction
θ_P	angular coordinate
$\dot{\theta}_P$	angular velocity
M_P	number of contacts of particle P
Q	number of particle in contact with P
$(F_n)_{PQ}$	normal force at this contact
$(F_s)_{PQ}$	shear force at this contact

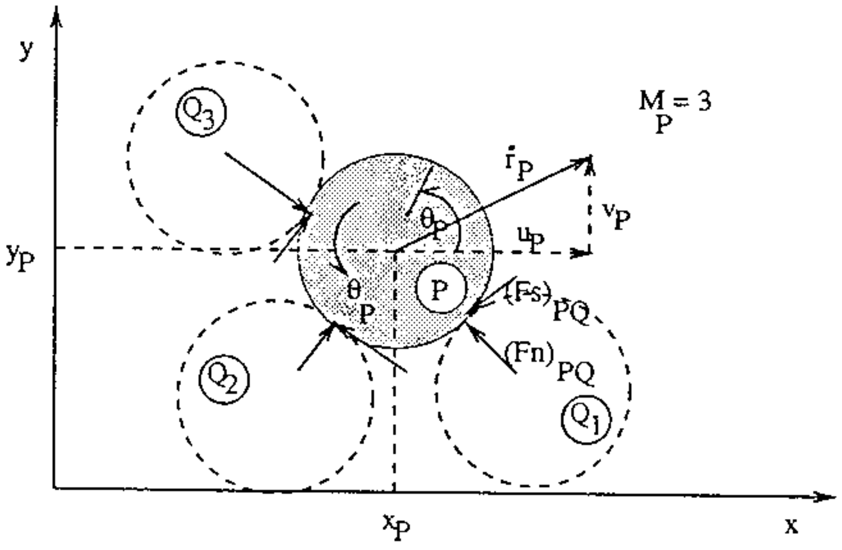

Figure 2.4. Description of the particle

Wall Definition

Each wall is described by the following set of informations (Figure 2.5):

W	number of wall
x_W	x-coordinate of wall reference point P_W
y_W	y-coordinate of wall reference point P_W
θ_W	angle between wall and x-axis
h_1	distance from P_W to the wall left end
h_2	distance from P_W to the wall right end
u_W	velocity of wall (P_W) in x-direction
v_W	velocity of wall (P_W) in y-direction
$\dot{\theta}_W$	angular velocity of the wall (about P_W)

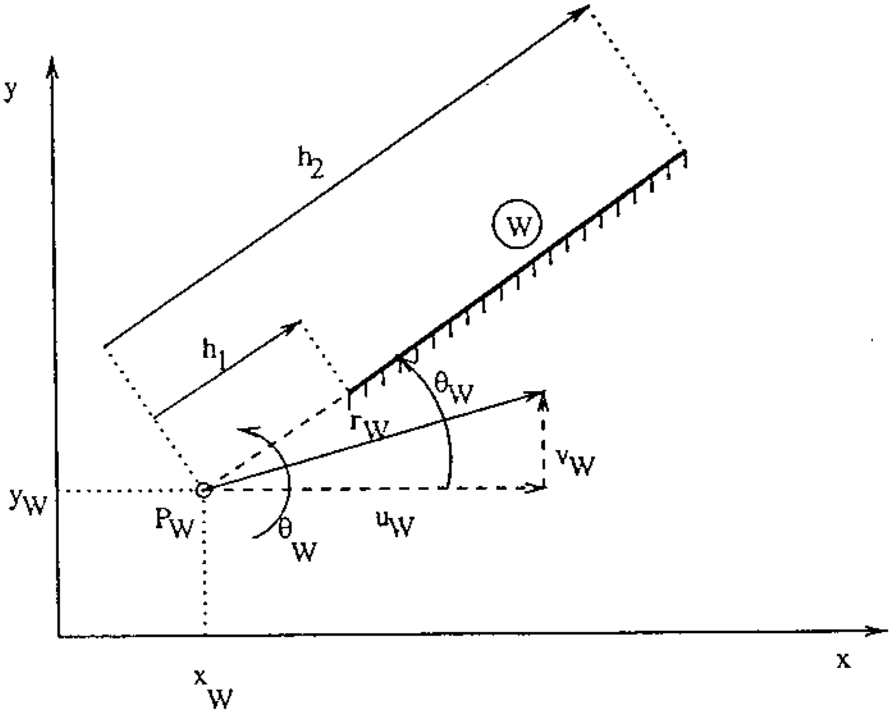

Figure 2.5. Description of the wall

2.2.3 Automatic Generation of Initial and Boundary Conditions

For the special systems such as rectangular wall bounded system and uniform rectilinear flow, the parameters defining the problem are read from the approppriate input file. Random initial conditions are automatically generated, and appropriate boundary conditions are automatically set up.

Rectangular Wall Bounded System

The problem specification is read from the file 'DIN.BOX'. In that file, user specifies number of particles N, concentration C and ratio of box width to length b/a. The box dimensions a and b can then be found using the relation

$$a = r\sqrt{\frac{N\pi}{(b/a)C}}, \qquad b = a(b/a) \tag{2.2}$$

The random initial condition is generated in two steps (Figure 2.6). First, the loose random packing is generated by placing particles randomly in the bigger box with the same shape ratio. The dimensions a_o and b_o of this box are chosen such that given number of particles divided by box area produces concentration $C_o = 0.4$. Secondly, this box is compressed mechanically by letting all walls move inwards with constant velocity for sufficient number of time steps (usually 1000) until the desired box dimensions a, b (and hence the concentration C) are obtained.

The boundary conditions (wall motion) are read from input file 'DIN.BCS', formatted in the same way as for the general system.

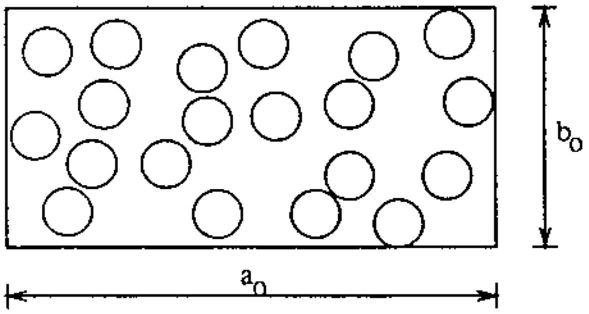

a) particles placed randomly, C=C =0.4

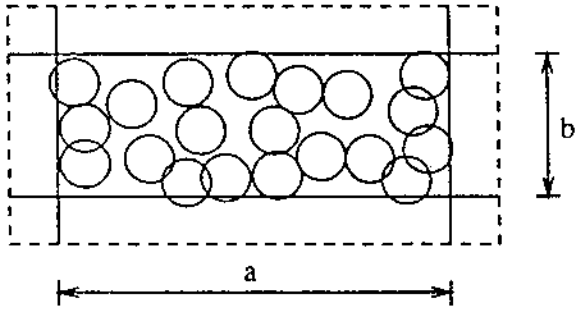

b) assembly compressed mechanically to
specified concentration C

Figure 2.6. Automatic generation of random initial conditions for rectangular wall bounded system

Uniform Rectilinear Flow

For the Couette or channel flow, the problem specification is read from the file 'DIN.CHN'. In that file, user specifies "flow driver" (U_o, g and α_o), the width of channel b, separation of boundary particles s_w (for "bumpy wall"), approximate ratio of channel width to calculation cell length b/a and approximate concentration C. For the case of flat wall, the specified values of C and b/a are exact. For the case of "bumpy" walls specified values of C and b/a have to be slightly adjusted in order to place boundary particles periodically. From these values, number of particles N is determined. Initial condition is generated in the manner similar to the one described in previous section for wall bounded system. The difference is that only the width of the box is extended such that loose random packing can be fitted in, and this assembly is then mechanically compressed by inward motion of two rigid walls.

For the chute flow, the problem specification is read from the file 'DIN.CHT'. In that file, user specifies the inclination angle of chute β_o, width of calculation cell a and number of particles N. The configurational difference with channel and Couette flow is that only one (bottom) wall is physically present. This allows for simpler generation of initial condition. Since no constraint is posed for loose random packing, mechanical compression is not necessary.

2.3 Calculation Cycle

The term calculation cycle refers here to the set of calculations performed during one time step of simulation. In its most basic form, the calculation cycle includes routines to search for all existing contacts, to calculate the forces at all contacts from the force-displacement law and to integrate equations of motion for all particles to obtain new positions and velocities. In addition, the calculation cycle may include routines that handle periodic boundary conditions, update statistical summations etc., depending on the version of the model. In the program, these routines are arranged in subroutine CYCLE which is called by main program thousands of times as the simulation proceeds.

The flow chart of subroutine CYCLE is shown in Figure 2.7.

2.3.1 Search Procedure

The process of search for contacts between the particles is potentially the most time consuming part of the simulation. The search strategy used in all soft-particle models is of "detector" type, i.e. the contact is registered when an overlap between two particles is detected. The simplest method of global search is to check for an overlap between all pairs of particles. However, for large number of particles N this method requires $N(N-1) \approx N^2$ comparisons, what becomes prohibitively time consuming. Therefore, the more efficient search procedure is devised, based on the idea of "neighbourhood search". This idea was introduced in the early years of molecular dynamics studies and is used in most of existing granular flow simulations.

The other method for improving efficiency of search procedure would be to keep short list of neighbors for each particle, and to search for contacts only among these neighbors. This list would not have to be updated every time step. However, this improvement is not implemented in the present model yet.

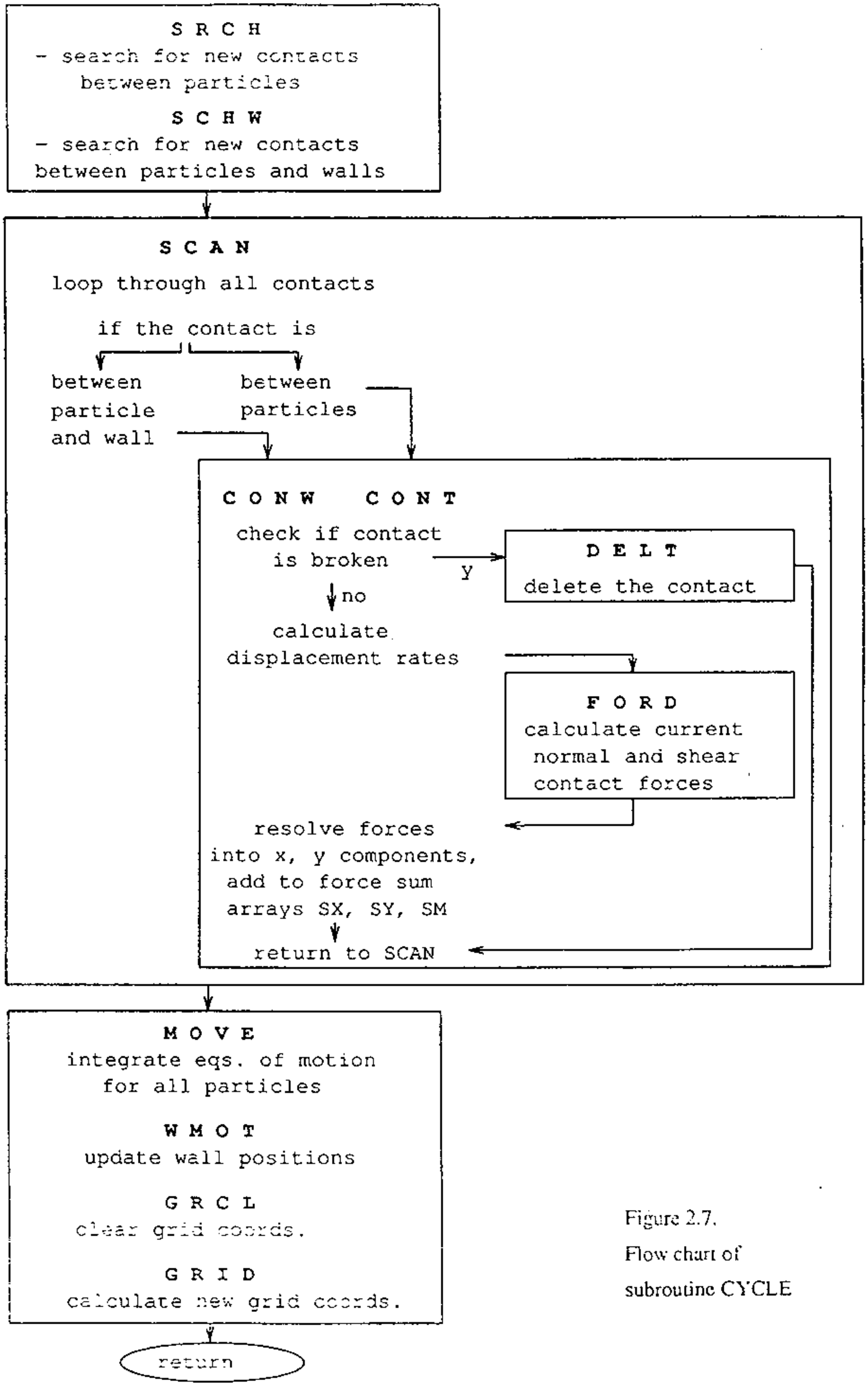

Figure 2.7.
Flow chart of
subroutine CYCLE

Grid System

In order to define a neighbourhood about a particle, a rectangular grid is superimposed onto a space occupied by particles. The size of cells is chosen such that only one particle center may occupy a cell at any given time. This rule implies cell $\leq R\sqrt{2}$ for uniform disks of radius R (Hopkins (1987)). For simplicity, in the present model the cell size is chosen to be equal to particle radius (cell=R). In this case, the area that needs to be searched for contacts of a given particle consists of 5^2-1 cells surrounding the cell occupied by the particle.

The grid is imposed onto a flow domain of dimensions (a,b) with the coordinate system centered at the center of flow domain. Number of cells in x and y directions is computed as

$$\mathrm{NX} = 2(\mathrm{int}(\frac{a}{2R}) + 2); \qquad \mathrm{NY} = 2(\mathrm{int}(\frac{b}{2R}) + 2) \tag{2.1}$$

such that grid fills an area at least 2 cells wider at each side than the actual physical space occupied by particles. This criterion ensures that search area around a given cell is always fully covered by grid system. Note also that NX and NY are always even. Particle I is assigned grid coordinates IX(I) and IY(I) as

$$\mathrm{IX(I)} = \mathrm{NX}/2 + \mathrm{int}(\mathrm{X(I)}/\mathrm{R}) + 1 \tag{2.2}$$

$$\mathrm{IY(I)} = \mathrm{NY}/2 + \mathrm{int}(\mathrm{Y(I)}/\mathrm{R}) + 1 \tag{2.3}$$

Two dimensional array NGR(K,L) is used to store number of particle I in the appropriate cell (address of the particle):

$$\mathrm{NGR(IX(I), IY(I))} = \mathrm{I} \tag{2.4}$$

These arrays provide means for finding the grid location of a particle and searching for contacts with its neighbours. The features of the grid system described above are shown in Figure 2.8.

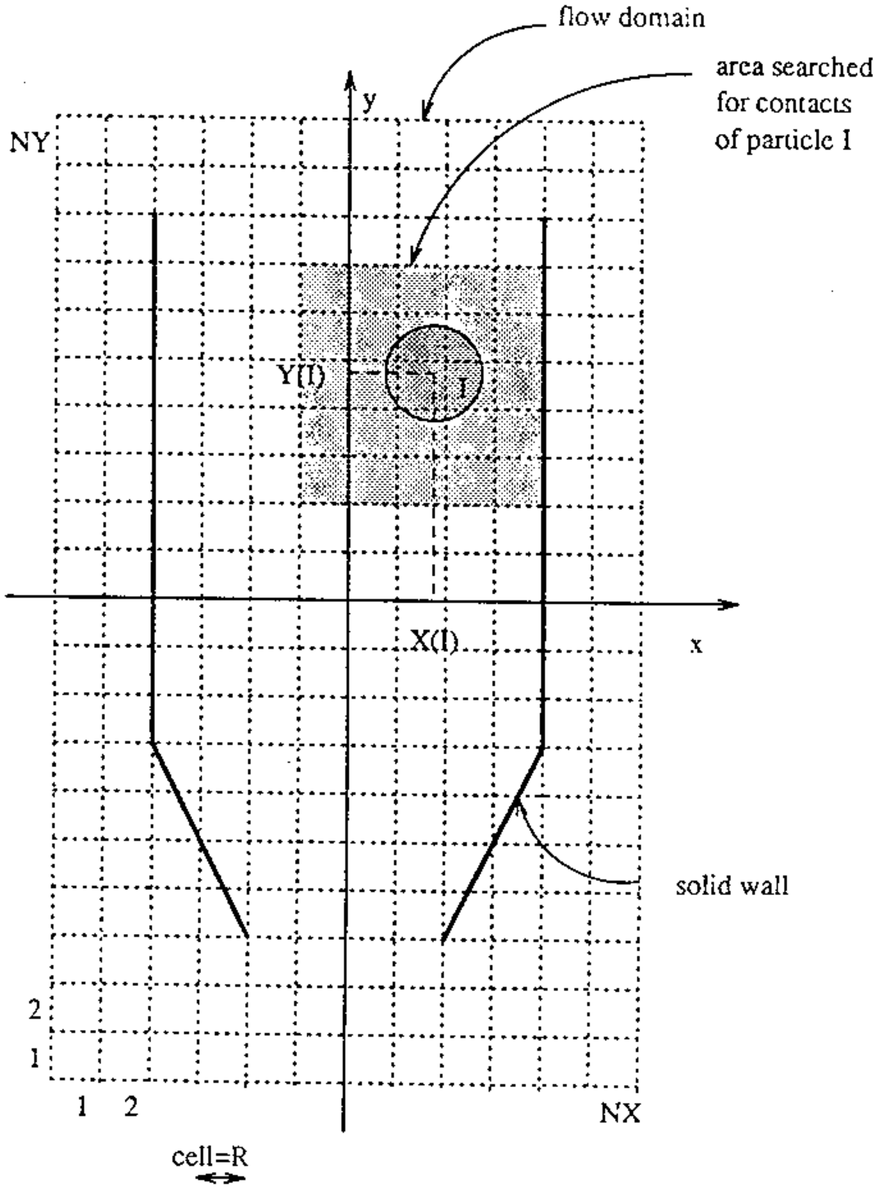

IX(I)=NX/2+INT(X(I)/R)+1

IY(I)=NY/2+INT(Y(I)/R)+1

NGR(IX(I),IY(I))=I

Figure 2.8. Grid System

Search for Contacts Between Particles

The search for new contacts between particles is performed in subroutine SRCH. Only $5^2 - 1$ cells around the particle A are searched. If particle B is found to be in one of these cells, the contact is detected if

$$s = \sqrt{(x_A - x_B)^2 + (y_A - y_B)^2} \leq 2\mathrm{R} \tag{2.5}$$

If the new contact is found, it is added to list of contacts of particle A, and the search is continued.

Search for Contacts Between Particles and Walls

The search for new contacts with walls is performed in subroutine SCHW. Since the number of walls NW is usually small, the check is made for possible contacts between all particles and all walls.

The contact between particle A and wall W is shown in Figure 2.10. The coordinates of the center of particle are (x_A, y_A). Wall W is defined by coordinates of the wall reference point (x_W, y_W) and angle θ_W with respect to x-axis. The distances between particle center and wall reference point in directions parallel to the wall and perpendicular to the wall are denoted by s_H and s_V, respectively. From geometrical considerations s_H and s_V are found to be

$$s_H = (x_A - x_W)\cos\theta_W + (y_A - y_W)\sin\theta_W \tag{2.6}$$

$$s_V = -(x_A - x_W)\sin\theta_W + (y_A - y_W)\cos\theta_W \tag{2.7}$$

The contact is detected if

$$h_1 \leq s_H \leq h_2 \quad \text{and} \quad 0 \leq s_V \leq \mathrm{R} \tag{2.8}$$

If the new contact is found, it is added to list of contacts of particle A, and the search is continued.

2.3.2 Contact Between Particles

The calculation of force at the contact between two particles is performed in subroutine CONT which is called by subroutine SCAN.

The contact of two discs, A and B, is shown in Figure 2.9. The position vectors of centers of disks A and B are represented as $\mathbf{r}_A = (x_A, y_A)$, $\mathbf{r}_B = (x_B, y_B)$. The velocity vectors of centers of disks A and B are represented as $\dot{\mathbf{r}}_A = (u_A, v_A)$, $\dot{\mathbf{r}}_B = (u_B, v_B)$, and the angular velocities are $\dot{\theta}_A$ and $\dot{\theta}_B$, taken positive in counterclockwise direction. The unit vector $\mathbf{k}$ is defined to be pointing from the center of disc A to the center of disc B and the unit vector $\mathbf{t}$ is obtained by a counterclockwise rotation of $\mathbf{k}$ through 90°, i.e.

$$\mathbf{k} = \frac{\mathbf{r}_B - \mathbf{r}_A}{|\mathbf{r}_B - \mathbf{r}_A|} = (\cos\alpha, \sin\alpha); \qquad \mathbf{t} = (-\sin\alpha, \cos\alpha) \tag{2.9}$$

Points P_A and P_B are defined as the points of intersection of the line connecting the disc centers with the boundaries of disks A and B, respectively. The relative displacement at the contact point C is determined by integration of the relative velocity. The relative velocity at the contact is defined as the relative velocity of point P_A with respect to P_B, which can be expressed as

$$\mathbf{V}_{AB} = (\dot{\mathbf{r}}_A - \dot{\mathbf{r}}_B) + \mathrm{R}(\dot{\theta}_A + \dot{\theta}_B)\hat{\mathbf{t}} \tag{2.10}$$

The relative displacement rates in normal and tangential direction $\dot{n}$ and $\dot{q}$ are the projections of $\mathbf{V}_{AB}$ onto $\mathbf{k}$ and $\mathbf{t}$, respectively:

$$\dot{n} = \mathbf{V}_{AB} \cdot \mathbf{k} = (u_A - u_B)\cos\alpha + (v_A - v_B)\sin\alpha \tag{2.11}$$

$$\dot{q} = \mathbf{V}_{AB} \cdot \mathbf{t} = -(u_A - u_B)\sin\alpha + (v_A - v_B)\cos\alpha + \mathrm{R}(\dot{\theta}_A + \dot{\theta}_B) \tag{2.12}$$

The contact force calculation is performed next, by calling subroutine FORD. The displacement rates $\dot{n}$ and $\dot{q}$ obtained above are input for contact force calculation in FORD, and the output are the values of current forces in normal and tangential directions S_n and S_s.

By the sign convention, forces S_n and S_s are positive in directions opposite to k and **t**, respectively. The x and y components of forces and the moment acting on the particle A are then calculated as

$$(F_x)_A = -(S_n \cos\alpha - S_s \sin\alpha) \tag{2.13}$$

$$(F_y)_A = -(S_n \sin\alpha + S_s \cos\alpha) \tag{2.14}$$

$$M_A = -S_s\mathrm{R} \tag{2.15}$$

Forces and moment acting on particle B are

$$(F_x)_B = -(F_x)_A; \qquad (F_y)_B = -(F_y)_A; \qquad M_B = M_A \tag{2.16}$$

These forces are added to arrays SX, SY and SM containing partial sum of forces and moments acting on each particle. Once the forces and moment acting on the particle from all its contacts are found, the values contained in these arrays become the resultant forces ΣF_x and ΣF_y and resultant moment ΣM acting on the particle, which are used to calculate motion of the particle.

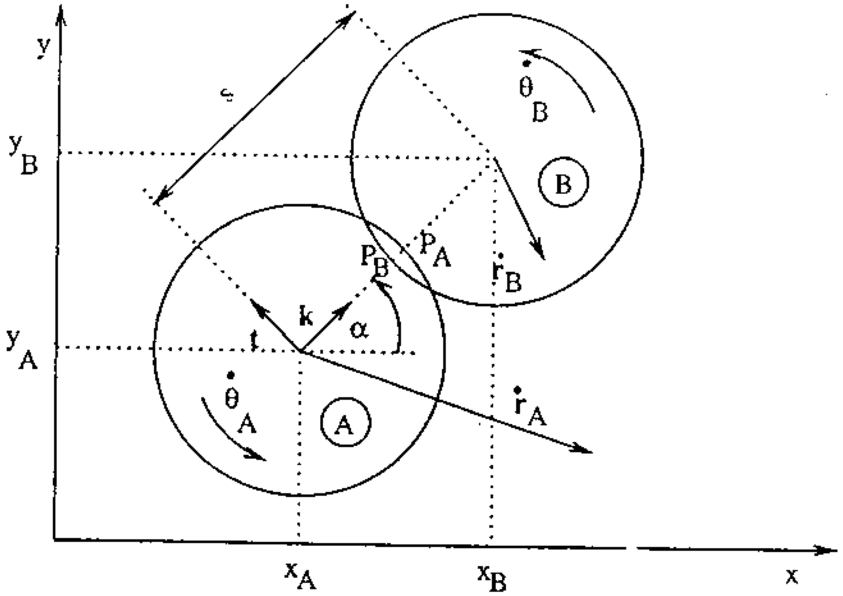

Figure 2.9.a: Contact between two particles

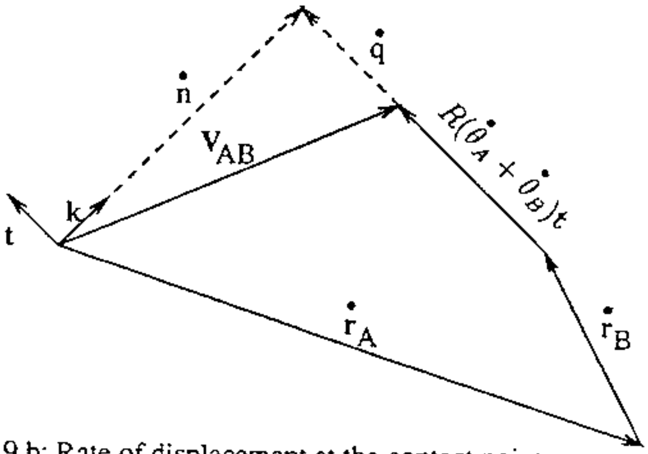

Figure 2.9.b: Rate of displacement at the contact point

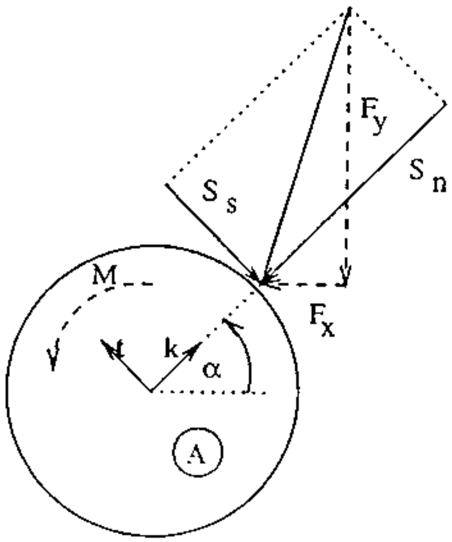

Figure 2.9.c: Forces acting on particle A

2.3.3 Contact Between Particle and Wall

The calculation of force at the contact between particle and wall is performed in subroutine CONW, which is called by subroutine SCAN.

The contact between particle A and wall W is shown in Figure 2.10. The position vector of particle A is $\mathbf{r}_A = (x_a, y_A)$, the velocity vector of its center is $\dot{\mathbf{r}}_A = (u_A, v_A)$, and the angular velocity is $\dot{\theta}_A$, taken as positive in counterclockwise direction. Wall W is defined by coordinates of its reference point $\mathbf{r}_W = (x_W, y_W)$ and the angle with respect to x-axis θ_W. The motion of wall is defined by velocity of reference point $\dot{\mathbf{r}}_W = (u_W, v_W)$ and the angular velocity about reference point $\dot{\theta}_W$. The unit vector k is defined to be pointing from the center of particle to the contact point, thus being perpendicular to the wall. Hence, $\mathbf{k} = (\sin\theta_W, -\cos\theta_W)$. The unit vector t is obtained by a counterclockwise rotation of k through 90°, i.e. $\mathbf{t} = (\cos\theta_w, \sin\theta_w)$.

The relative velocity $\mathbf{V}_{AW}$ at the contact point C is defined as the relative velocity of point P_A on the particle and point P_W on the wall. The velocity of point P_A is

$$\mathbf{V}_A = \dot{\mathbf{r}}_A + \mathrm{R}\dot{\theta}_A\mathbf{t} \tag{2.17}$$

and the velocity of point P_W is

$$\mathbf{V}_W = \dot{\mathbf{r}}_W - s_H\dot{\theta}_W\mathbf{k} \tag{2.18}$$

where s_H is given by equation (2.6). Hence,

$$\mathbf{V}_{AW} = \mathbf{V}_A - \mathbf{V}_W = \dot{\mathbf{r}}_A - \dot{\mathbf{r}}_W + \mathrm{R}\dot{\theta}_A\mathbf{t} + s_H\dot{\theta}_W\mathbf{k} \tag{2.19}$$

The relative displacement rates in normal and tangential direction $\dot{n}$ and $\dot{q}$ are the projections of $\mathbf{V}_{AW}$ onto k and t, respectively:

$$\dot{n} = \mathbf{V}_{AW}\cdot\mathbf{k} = (u_A - u_W)\sin\theta_W - (v_A - v_W)\cos\theta_W - s_H\dot{\theta}_W \tag{2.20}$$

$$\dot{q} = \mathbf{V}_{AW} \cdot \mathbf{t} = (u_A - u_W)\cos\theta_W + (v_A - v_W)\sin\theta_W + \mathrm{R}\dot{\theta}_A \tag{2.21}$$

The contact force calculation is performed next, by calling subroutine FORD. The displacement rates $\dot{n}$ and $\dot{q}$ obtained above are input for contact force calculation in FORD, and the output are the values of current forces in normal and tangential directions S_n and S_s.

By the sign convention, forces S_n and S_s are positive in directions opposite to **k** and **t**, respectively. The x and y components of forces and the moment acting on the particle A are then calculated as

$$(F_x)_A = -(S_n \sin\theta_w + S_s \cos\theta_w) \tag{2.22}$$

$$(F_y)_A = -(-S_n \cos\theta_w + S_s \sin\theta_w) \tag{2.23}$$

$$M_A = -S_s\mathrm{R} \tag{2.24}$$

The forces on the wall are

$$(F_x)_W = -(F_x)_A; \qquad (F_y)_W = -(F_y)_A; \qquad M_W = -S_n s_H \tag{2.25}$$

The forces acting on the particle from this contact are added to arrays SX, SY and SM containing partial sums of forces and moments acting on the particle. The forces and the moment acting on the wall from this contact are added to arrays SWX, SWY and SWM containing partial sums of forces and moments acting on the wall.

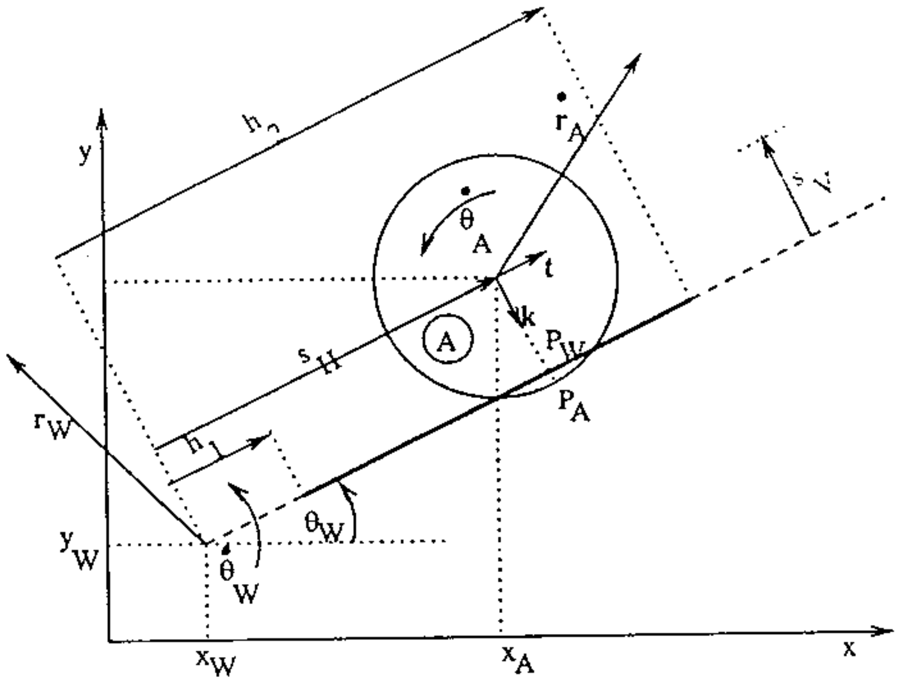

Figure 2.10.a: Contact between particle and wall

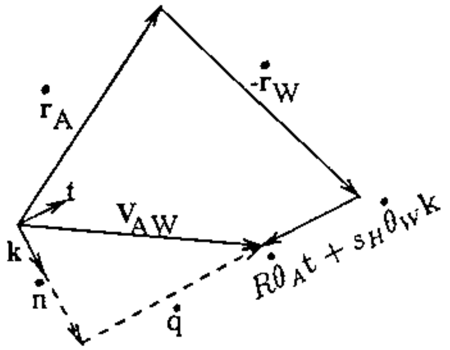

Figure 2.10.b: Rate of displacement at the contact point

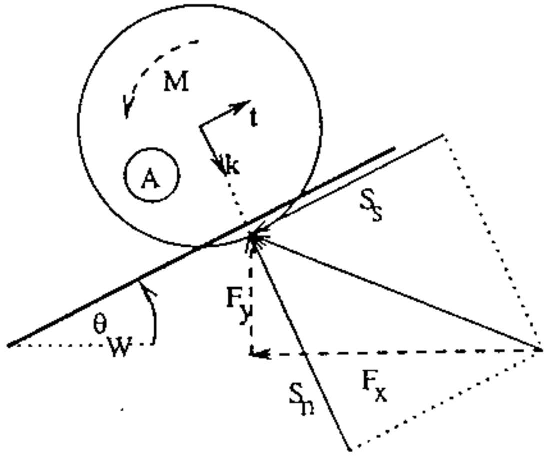

Figure 2.10.c: Forces acting on particle A

2.3.4 Contact Force Model

The contact force calculation is performed in subroutine FORD.

The contact force model (force-displacement law) currently implemented in model DINAMO is the same as the one used in model BALL by Cundall and Strack (1979a, 1979b). This particular contact force model is investigated in detail for binary contacts (collisions) in Appendix A. The schematic representation of this contact force model is shown in Figure 2.11.

The force in normal direction is modeled as viscoelastic (damped harmonic oscillator). It consists of elastic (spring) contribution and viscous damping (dashpot) contribution. The force in tangential direction is modeled as viscoelastic below the friction limit, and frictional at the friction limit. The friction limit is assumed to be given by Mohr-Coulomb law.

The normal particle stiffness k_n is an input constant of this model, which is in principle related to particle's modulus of elasticity E. It must be selected with some care to be sufficiently large to be able to balance inertia and body forces in the system without creating unrealistically large overlaps (deformations). The tangential particle stiffness k_s is in principle related to particle's shear modulus of elasticity G. Therefore, its range of values is restricted to $\frac{2}{3}k_n < k_s < k_n$ corresponding to limited range of values of the material Poisson's ratio.

The effective contact stiffnesses in normal and tangentional directions K_n and K_s are obtained from particle stiffnesses k_n and k_s. Using the analogy with springs connected in series, the effective stiffnesses for identical particles are $K_n = k_n/2$ and $K_s = k_s/2$.

The relative displacements and displacement rates derived from kinematics are used in the force-displacement law described above.

Sign(-1) = -1   Sign [illegible]

The increments of the normal and shear spring forces ΔF_n and ΔF_s are

$$\Delta F_n = K_n \dot{n} \Delta t; \qquad \Delta F_s = K_s \dot{q} \Delta t \tag{2.26}$$

To obtain the current spring forces the force increments ΔF_n and ΔF_s are added into the sum of all force increments, F_n and F_s, determined for previous time steps:

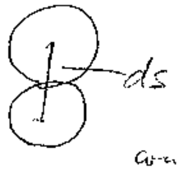

$$(F_n)_N = (F_n)_{N-1} + \Delta F_n \tag{2.27}$$

$$(F_s)_N = (F_s)_{N-1} + \Delta F_s \tag{2.28}$$

ds < r
compress.

Damping

The contact damping operates on the relative velocities at the contacts. The damping forces D_n and D_s are proportional to components of relative velocities $\dot{n}$ and $\dot{q}$:

$$D_n = C_n \dot{n}; \qquad D_s = C_s \dot{q} \tag{2.29}$$

where C_n and C_s are (dimensional) coefficients of viscous contact damping. These coefficients are related to dimensonless damping coefficients normal and tangential directions ζ_n and ζ_s as

$$C_n = 2\zeta_n \sqrt{m K_n}; \qquad C_s = 2\zeta_s \sqrt{m K_n} \tag{2.30}$$

The damping coefficient ζ_n is related to particle coefficient of restitution ϵ. It is shown in Appendix A on the basis of theoretical solution for binary contact (collision) that an explicit relationship between normal damping and coefficient of restitution is

$$\zeta_n = \frac{-\ln \epsilon}{\sqrt{\pi^2 + \ln^2 \epsilon}} \tag{2.31}$$

The shear damping coefficient ζ_s is assumed in this model to be constant which can be independently selected. Its value is usually selected to be of order of ζ_n, or, in some cases, to be equal to zero.

Friction

A Coulomb-type friction law is incorporated as follows. The magnitude of shear force found from equation (2.28) can not exceed the maximum possible value $(F_s)_{max}$ defined as

$$(F_s)_{max} = \mu F_n \tag{2.32}$$

where μ is the interparticle friction coefficient. If the absolute value of $(F_s)_N$ as found from equation (2.28) is larger than $(F_s)_{max}$, then $(F_s)_N$ is set equal to $(F_s)_{max}$, preserving the sign obtained from equation (2.28). In that case, the viscous damping in the shear direction is not applied, i.e. $D_s = 0$.

Total Forces

The total current forces in normal and tangential directions are

$$S_n = F_n + D_n; \qquad S_s = F_s + D_s \tag{2.33}$$

These forces are the output of subroutine FORD, and are returned to subroutine which has called it.

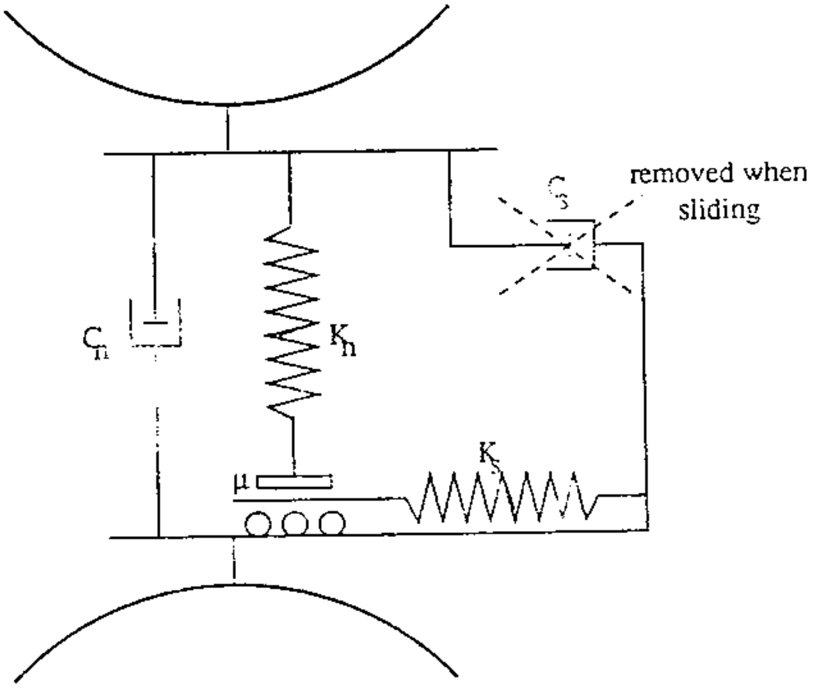

Figure 2.11. Contact force model

2.3.5 Motion

Once all resultant forces and moments acting on each particle are obtained, new velocities and positions of all particles are obtained by numerical integration of second Newton's law. These calculations are performed in subroutine MOVE.

Newton's second law for the linear motion applied to a particle is

$$m\ddot{\mathbf{r}} = \Sigma\mathbf{F} + m\mathbf{g} \tag{2.34}$$

where g is the acceleration vector due to the body force, i.e. gravity.

Newton's second law for the angular motion is

$$I\ddot{\theta} = \Sigma M \tag{2.35}$$

where I is the moment of inertia of the particle.

The time-centred finite-difference scheme is devised to allow explicit numerical integration of the above equations.

The current resultant force and the moment at time t_N are assumed to act on particle during the interval Δt from $t_{N-\frac{1}{2}}$ to $t_{N+\frac{1}{2}}$. Thus, assuming the accelerations $\ddot{\mathrm{r}}$ and $\ddot{\theta}$ to be constant over the time step Δt, integration of equations (2.34) and (2.35) lead to the following expressions for the velocities

$$(\dot{\mathrm{r}})_{N+\frac{1}{2}} = (\dot{\mathrm{r}})_{N-\frac{1}{2}} + (\frac{(\Sigma\mathrm{F})_N}{m} + \mathrm{g})\Delta t \tag{2.36}$$

$$(\dot{\theta})_{N+\frac{1}{2}} = (\dot{\theta})_{N-\frac{1}{2}} + \frac{(\Sigma M)_N}{I}\Delta t \tag{2.37}$$

The new values of velocities are used to update the positions and rotations of the particles by a further numerical integration

$$(\mathrm{r})_{N+1} = (\mathrm{r})_N + (\dot{\mathrm{r}})_{N+\frac{1}{2}}\Delta t \tag{2.38}$$

$$(\theta)_{N+1} = (\theta)_N + (\dot{\theta})_{N+\frac{1}{2}}\Delta t \tag{2.39}$$

Wall Motion

The motion of the walls is updated in subroutine WMOT. The new location of the wall is found from prescribed boundary conditions, i.e. velocity of wall reference point $\dot{\mathbf{r}}_W$ and the angular velocity $\dot{\theta}_W$ about this point. The new position of wall reference point is

$$(\mathbf{r}_W)_{N+1} = (\mathbf{r}_W)_N + (\dot{\mathbf{r}}_W)\Delta t \tag{2.40}$$

and the new angle with respect to x-axis is

$$(\theta_W)_{N+1} = (\theta_W)_N + (\dot{\theta}_W)\Delta t \tag{2.41}$$

Grid Coordinates

The old grid coordinates of particles are first cleared by subroutine GRCL, and new grid coordinates are calculated by subroutine GRID, according to (2.2) and (2.3).

These calculations complete full calculation cycle.

Chapter 3

Preliminary Results

In this chapter the preliminary results of the present numerical model are presented. These results include the nine-disc verification test, two illustrative examples of general flows, the slow deformation of material in a rectangular wall-bounded system and profiles of concentration and velocity in Couette and channel flows.

3.1 Nine Disc Test

In this section, the results of simple nine disc test reported by Cundall and Strack (1979) are quantitatively verified using the present model.

The assembly of nine discs is initially packed in regular square packing enclosed in a square formed by four rigid walls. The particle radius is 50 units and particle density is 1000 units. The problem was to evaluate the response of the assembly to uniform compression and distortion, examining in particular the contact force at one selected contact.

The results of the present model are shown in figures 3.1-3.5. The corresponding original figures from Cundall and Strack(1979) are reproduced for comparison.

Uniform Compression

The boundary condition for uniform compression is that the walls move inwards with constant velocity until 40 calculation cycles have been completed. The wall motion is stopped at that point, but the test is continued to observe the subsequent behavior of the contact force at contact C.

The display of the assembly and contact forces obtained by uniform compression is shown in Figure 3.1. The contact forces are represented as rectangles centered at the contact point, inclined in the direction of the force. The length of the rectangle is equal to the sum of particle radii and the width is proportional to the magnitude of contact force (scaled by maximum force in the assembly at that instant).

Figure 3.2. shows the effect of damping. The solid line corresponds to the case in which there is no damping. In the present model that implies $\epsilon = 0$, $\zeta_s = 0$. The dashed line corresponds to the nonzero damping. The values of damping parameters used in original test were not reported, and the value of $\epsilon = 0.75$ had to be guessed in present model to obtain the most similar results. It appears from the figure that damping does not affect the equilibrium value of the force, but does reduce the time needed to reach an equilibrium.

Figure 3.3. shows the effects of loading speed and particle stiffness. The normal and shear stiffness were $k_n = k_s =$1.35E+9 and $k_n = k_s =$1.50E+8 in figures 3.3.a. and 3.3.b, respectively. Two different loading sequences were performed: 40 cycles with velocity 0.12 and 120 cycles with velocity 0.04. The equilibrium value of the force is equal in both cases, but it appears that slower loading produces lower amplitude of damped oscillations. For larger stiffness (Figure 3.3.b), results of the present model ar somewhat different from the results of BALL. The reason for that is that in BALL, the damping coefficients are functions of stiffness and mass (Rayleigh damping) while in present model they are function of restitution coefficient only.

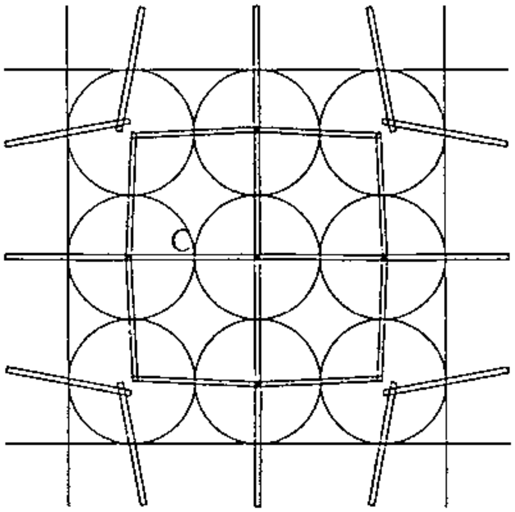

Figure 3.1. Nine disc test, uniform compression
Below: Figure 5 reproduced from Cundall and Strack (1979)

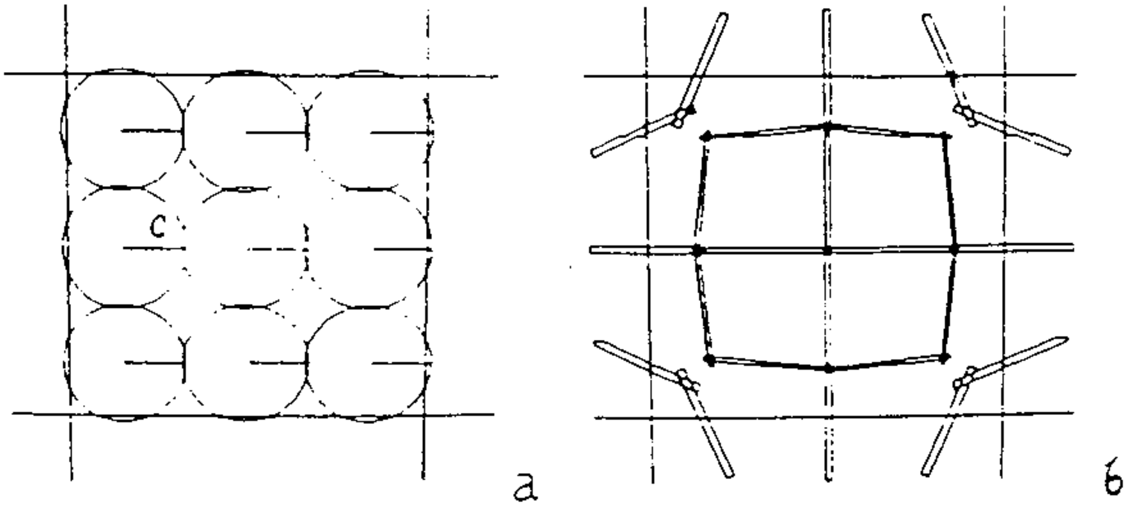

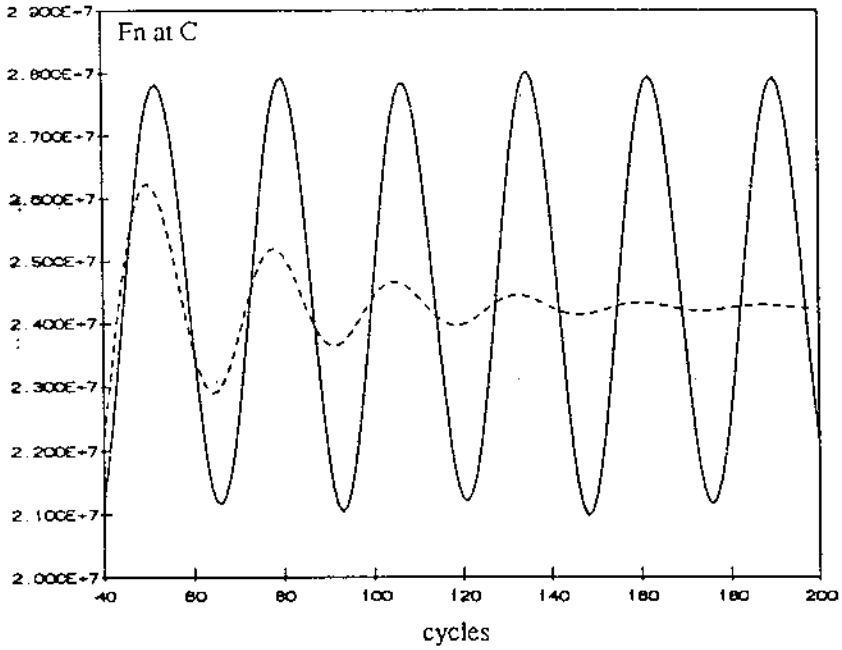

Figure 3.2. Force at contact C

Solid line: no damping, dashed line: contact damping.

Parameters: R=50, kn=ks=1.35E+9, dt=0.01525

Below: Figure 6 reproduced from Cundall and Strack (1979)

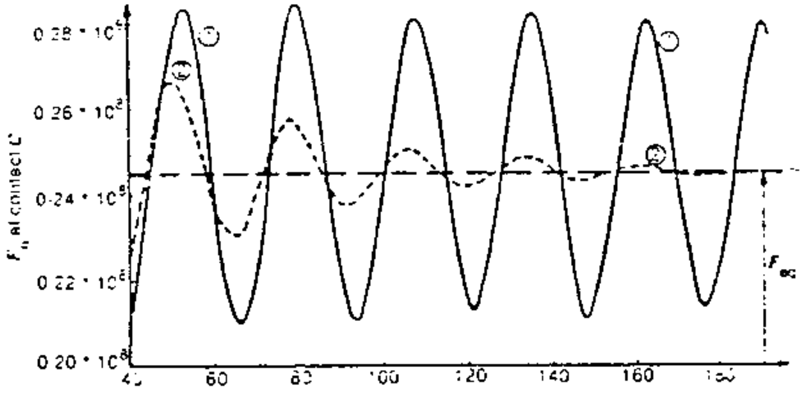

Cycles curve 1, no damping; curve 2, mass and stiffness damping

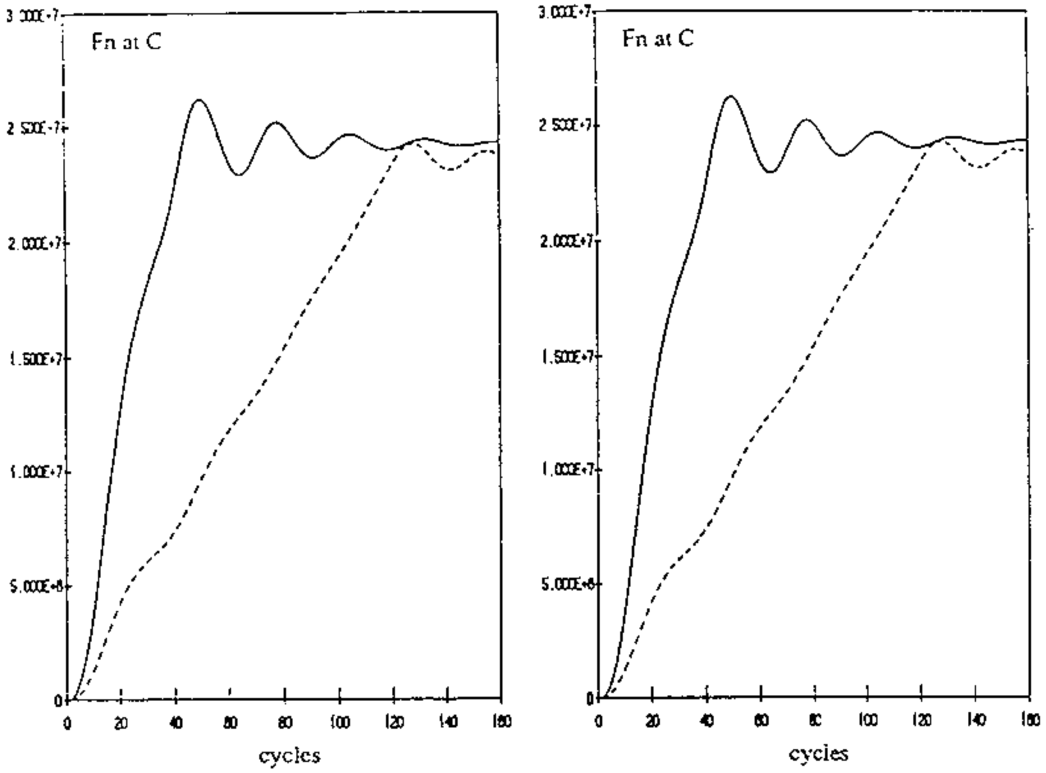

a] kn=ks=1.35E+9, dt=0.01525 b] kn=ks=1.50E+8, dt=0.04576

Figure 3.3. The effects of loading speed and particle stiffness

Solid line: loading for 40 cycles with inward wall velocities 0.12

Dashed line: loading for 120 cycles with inward wall velocities 0.04

Below: Figure 7 reproduced from Cundall and Strack (1979)

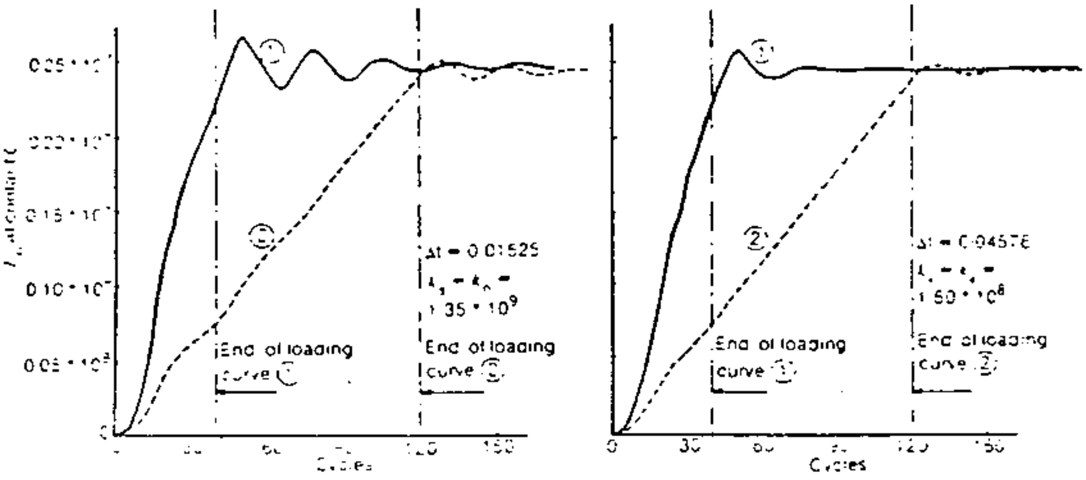

Distortion

The distortion test was not described very thoroughly in Cundall and Strack (1979). The probable loading sequence had to be reconstructed by examination of their results. The assembly was initially compressed for 4000 steps with velocity 0.12 to obtain value of the initial normal force of about 2.3E+9, almost 100 times larger than in previous test. The oscillations are then damped by not moving walls at all for another 1000 steps. After that, the constant volume distortion was created by rotating walls uniformly with angular velocity 0.0175 (this value was not reported bu Cundall and Strack, and was obtained by trial and error by comparing results). Figure 3.4 shows the configuration and the forces in the assembly after 500 time steps of distortion.

Figure 3.5. shows the effect of k_s/k_n ratio and friction angle ϕ (friction coefficient $\mu = \tan\phi$) on the development of both normal and shear forces atcontact C during distortion. The comparison with original figures is very good, although, again, there was no reference to values of damping coefficients. In present model $\epsilon = 0.2$ was used.

Figure 3.5.a shows very minor effect of ratio k_s/k_n for $\phi = 15^o$. The reason for this is that the slip sets very early, and the avlue of shear force is from then on determined solely by the normal force. For the case in Figure 3.5.b, however, where $\phi = 30^o$, the curves for $k_s/k_n = 2/3$ and $k_s/k_n = 1$ deviate significantly, since the shear stiffness controls the behavior over a longer portion of the test.

In conclusion to this section, it can be stated that the present model has successfully reproduced all of the original results reported by Cundall and Strack (1979).

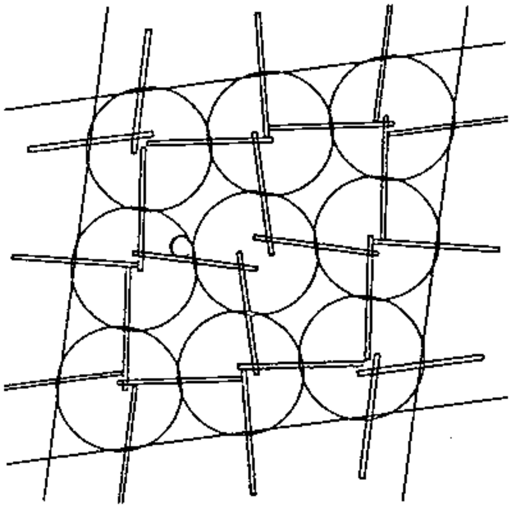

Figure 3.4. Nine disc test, distortion
Below: Figure 8 reproduced from Cundall and Strack (1979)

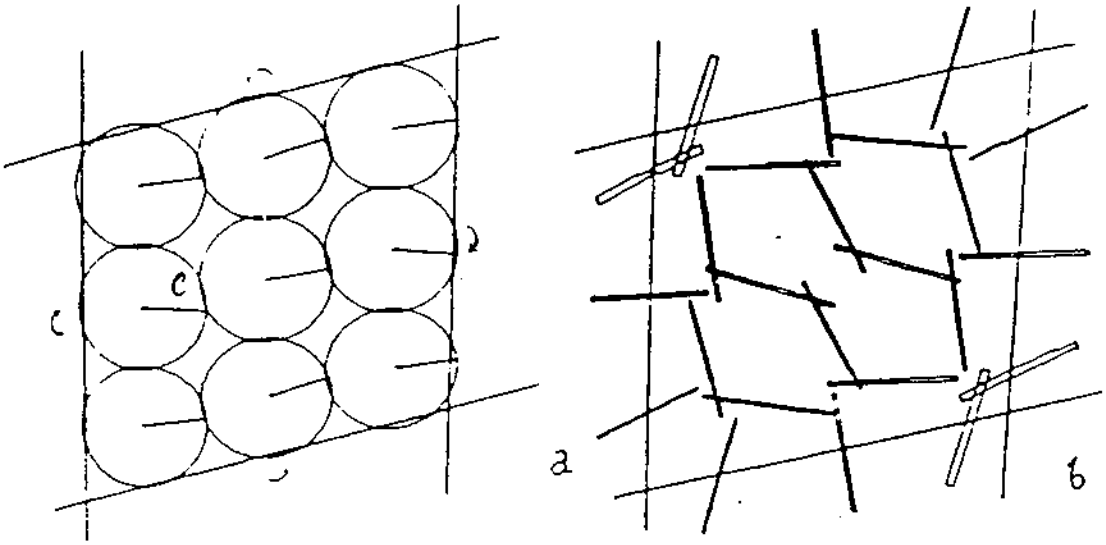

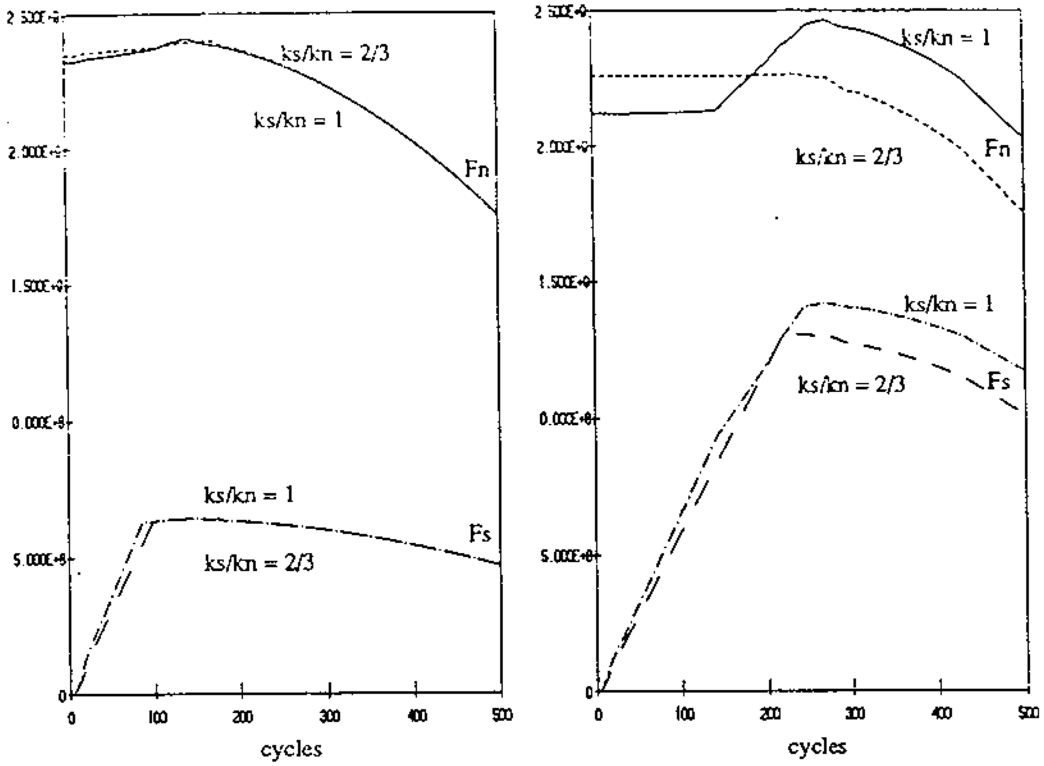

a] friction angle $\phi = 15°$ b] friction angle $o = 30°$

Figure 3.5. The effects of shear to normal stiffness ratio and friction angle in the distortion test

Below: Figure 7 reproduced from Cundall and Strack (1979)

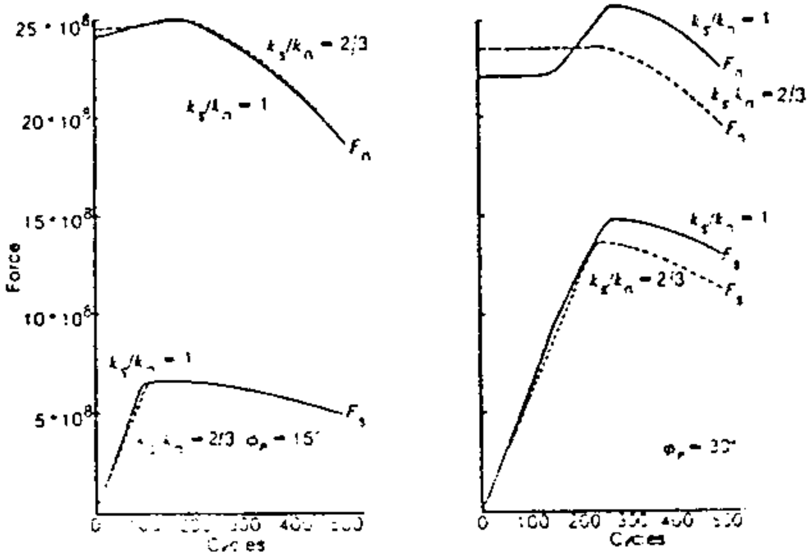

3.2 Bin Flow

Simulation of the bin flow of granular material was performed as one of two illustrative examples of the present model performance. The general version of the model was used. The behavior of the system is presented in suggestive graphical form by plotting selected frames at different stages of the simulation (Figure 3.7). This example was also shown in Walton (1982), and the results appear to be in good qualitative agreement.

For the general version of the model, the initial and boundary conditions are read from input files. The initial condition was generated in preliminary run in the following way. First, the rectangular area within the bin was packed by particles in loose random packing ($C = 0.4$) using simple supplementary program PACK. This was used as an initial condition for the preliminary run. The gravitational packing was then obtained by turning on the gravity in y-direction until the particles are settled down.

In the beginning of the actual run the bottom wall of the bin was suddenly removed and particles were able to flow through the opening and to eventually settle in the container below the bin. The whole run lasted for relatively short time (8000 time steps).

The details of the process can be followed by means of plotting instantaneous configuration, velocity and force plots at specifed times. One typical force plot (at t=4000dt) is shown in Figure 3.8, where the forces are plotted as rectangles described earlier in this chapter.

The parameters used for this run were: $R = .5$, $\rho_s = 1000$, $k_n = k_s$ =1E+8, $\epsilon = 0.8$, $\zeta_n = \zeta_s = 0.07085$, $\mu = 0.26795$, $g_y = -10$. The dimensions of walls are shown in Figure 3.6.

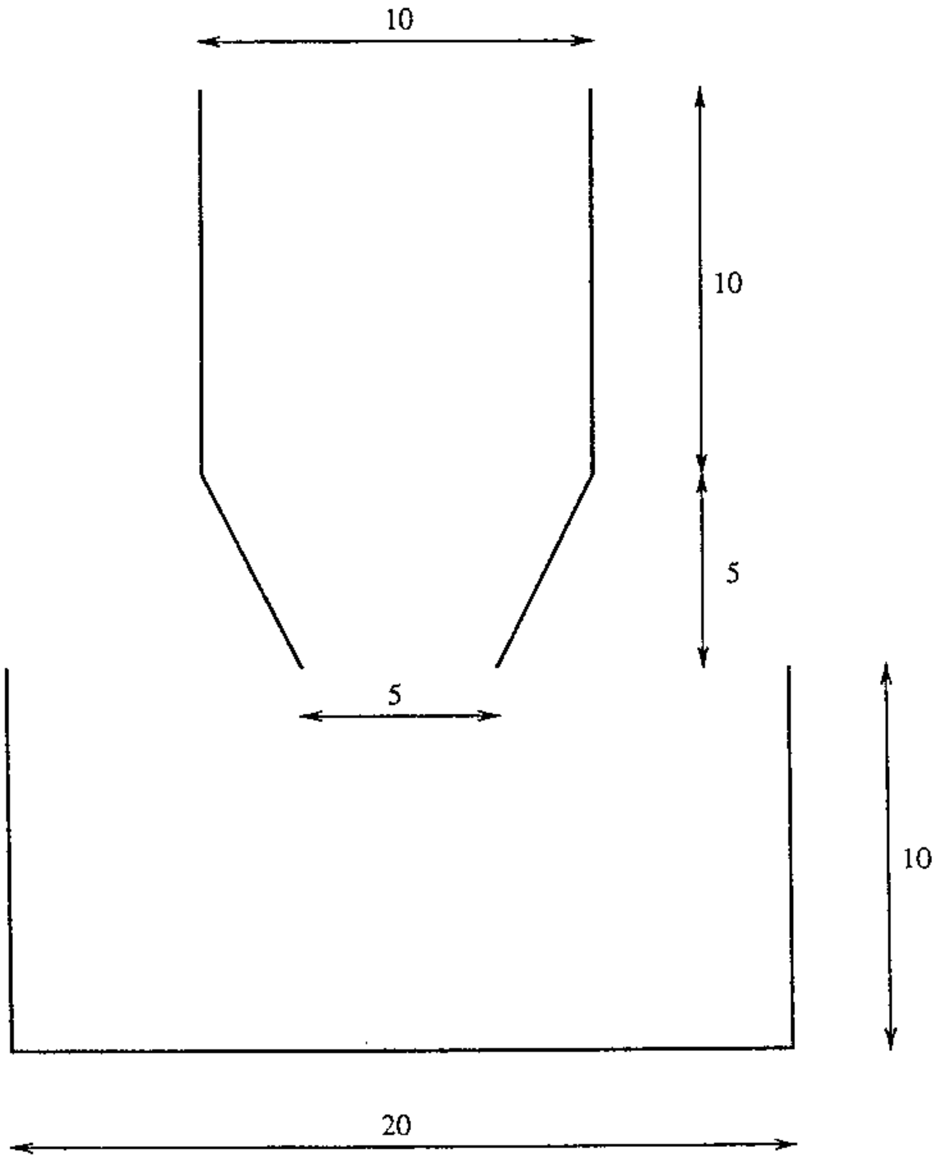

Figure 3.6. Dimensions of walls in bin problem

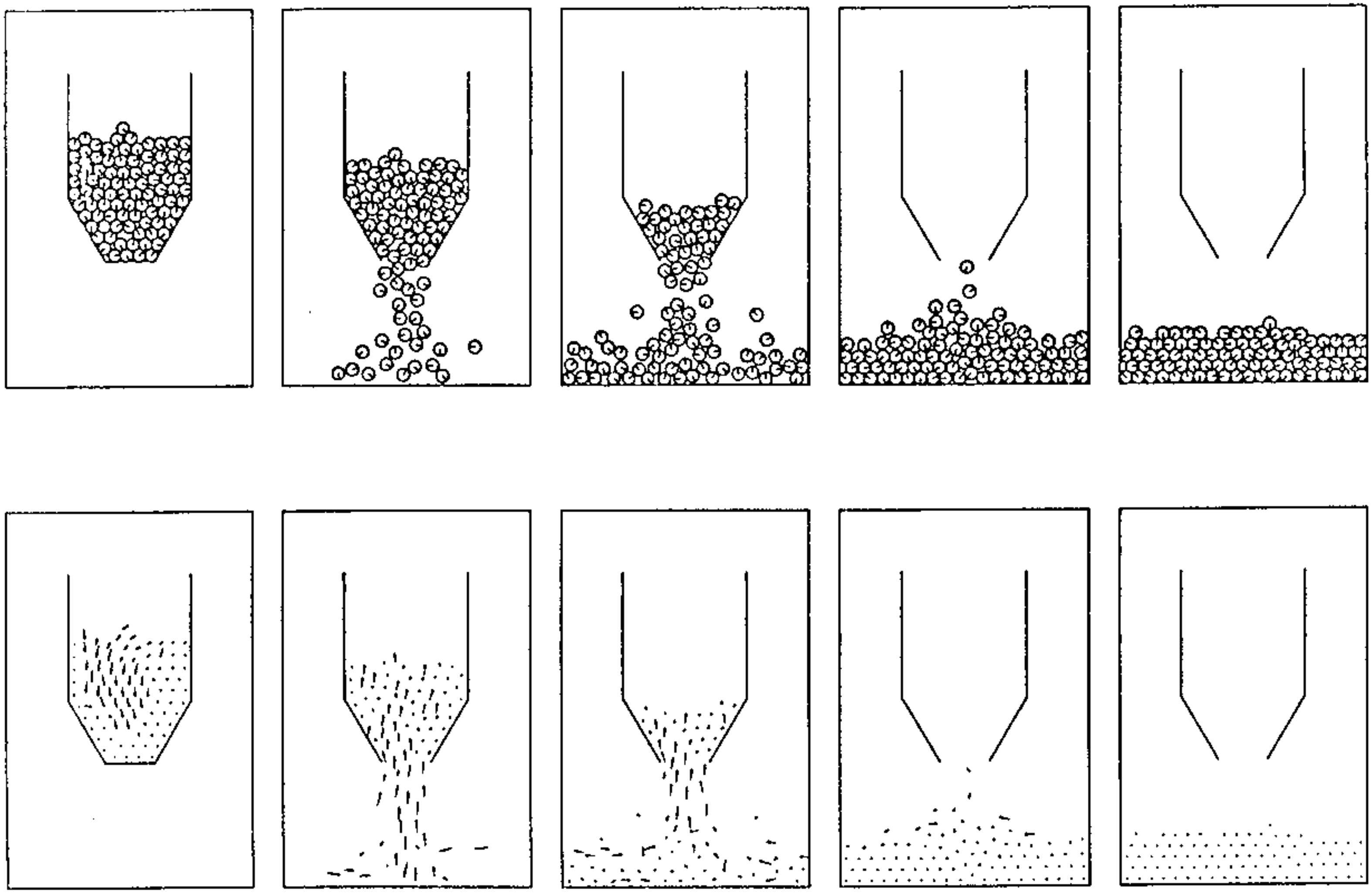

Figure 3.7. Simulation of the bin flow of granular material.

Frames are plotted at times t=0, 2000, 4000, 6000, 8000 time steps.

Top sequence shows configuration plots, bottom sequence shows velocity plots.

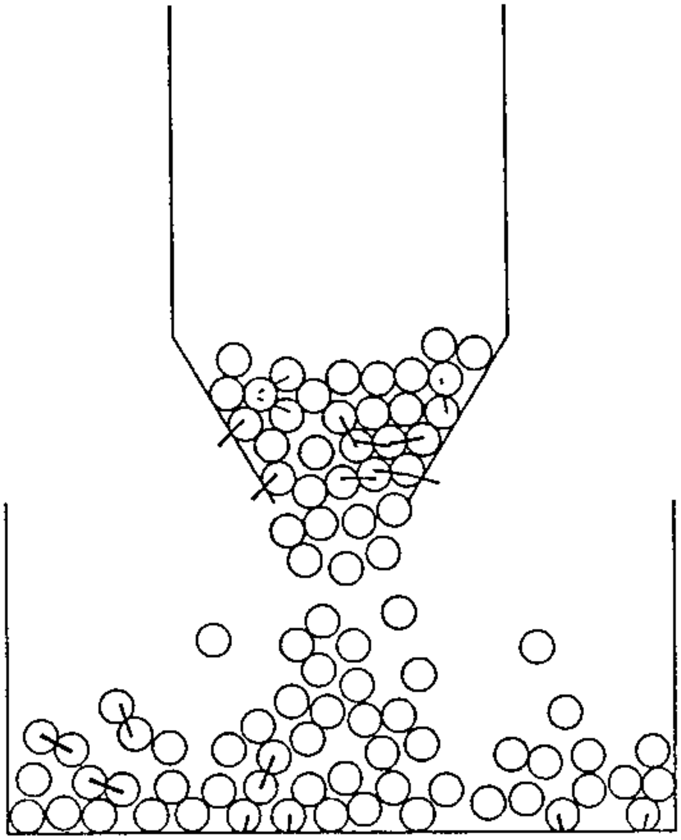

Figure 3.8. Force plot of bin flow at t=4000dt.

3.3 Flow Down the Cascade of Chutes

Simulation of the flow down the cascade of chutes is another illustrative example of model performance. This example was also shown in Walton (1982), but for much larger number of irregularly shaped particles. His study was motivated by practical interest in the problem of oil shale rubble.

The initial condition was created in the same way as already described for bin flow. The simulation begins by pulling up the wall on the right from particles. The further course of events is evident from figures 3.10.a. and 3.10.b., in which the configuration and velocity plots are shown every 2000 steps.

The parameters used for this run were: $R = .5$, $\rho_s = 1000$, $k_n = k_s = 1E+8$. $\epsilon = 0.8$, $\zeta_n = \zeta_s = 0.07085$, $\mu = 0.26795$, $g_y = -10$. The dimensions of walls are shown in Figure 3.9.

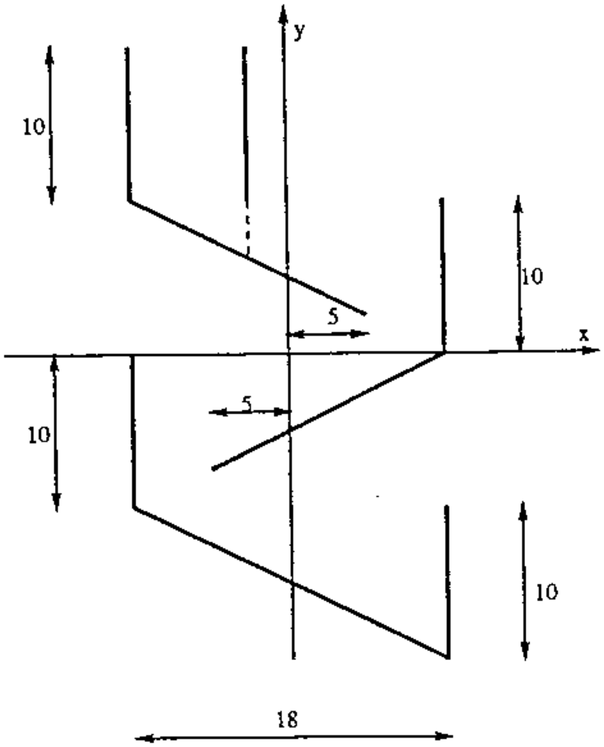

Figure 3.9. Wall dimensions for cascade problem

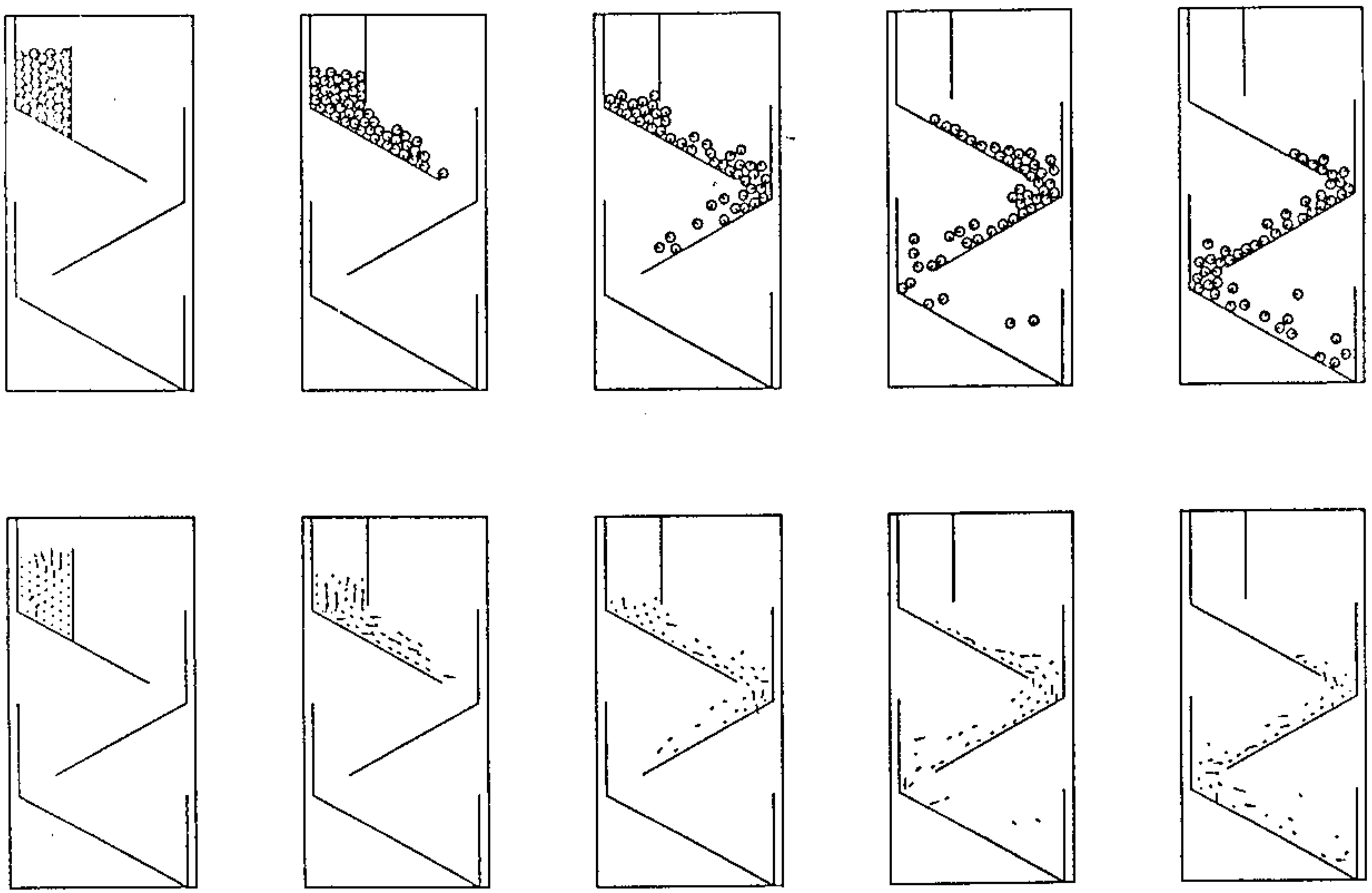

Figure 3.10.a. Simulation of the flow of granular material down the cascade of chutes.
Frames are plotted at times t=0, 2000, 4000, 6000, 8000 time steps.
Top sequence shows configuration plots, bottom sequence shows velocity plots.

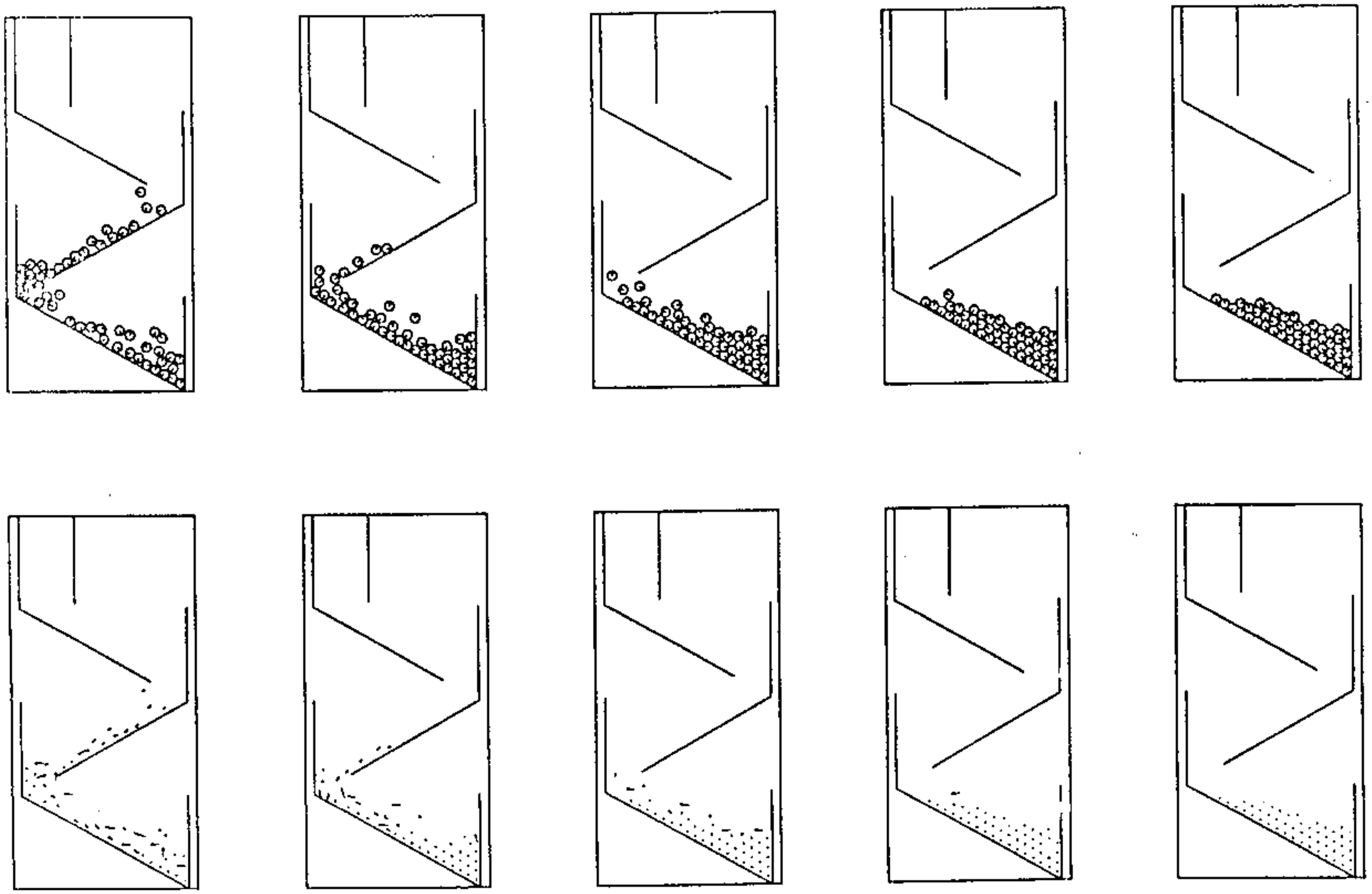

Figure 3.10.b. Simulation of the flow of granular material down the cascade of chutes.
Frames are plotted at times t=10000, 12000, 14000, 16000, 18000 time steps.
Top sequence shows configuration plots, bottom sequence shows velocity plots.

3.4 Wall Bounded System

In this section, the slow deformation of granular material in a rectangular wall-bounded "box" is simulated. The "wall-bounded" version of the model is used.

The experiment consists of simulation of the behavior of material subjected to specified loading sequence. The loading is prescribed in terms of wall velocities and rotations, what is perhaps the most primitive boundary control technique. The more advanced numerical models specialized for the slow material deformation (Cundall and Strack, Thornton) use more sophisticated boundary control techniques (stress-controlled, strain-controlled or servo-controlled boundary) to eliminate inhomogeneities caused by the presence of physical walls. These features have not been incorporated in present model yet. Therefore, no attempt has been made to perform physically significant numerical experiment with present model.

The results of one numerical run are reported here as an example. Number of particles is N=50, and initial concentration C=0.8. The initial condition is shown in Figure 3.11. It was obtained by mechanical compression of loose random packing for 1000 time steps, with another 3000 steps for relaxation (damping of oscillations). It should be noted that concentration is not exactly 0.8, because the total area of overlaps is not very small. The loading sequence consists of two parts. First, assembly is uniformly compressed for 10000 time steps with inward wall velocity of 0.5. The resulting configuration and contact forces are shown in Figure 3.12. Second, assembly is distorted for 5000 time steps with uniform angular velocity of walls about their centers of 0.1. The resulting configuration and contact forces are shown in Figure 3.13.

The parameters used for this run were: $R = 0.5$, $\rho_s = 1000$, $k_n = k_s = 1E+10$, $\epsilon = 0.8$, $\zeta_n = \zeta_s = 0.07085$, $\mu = 0.26794$.

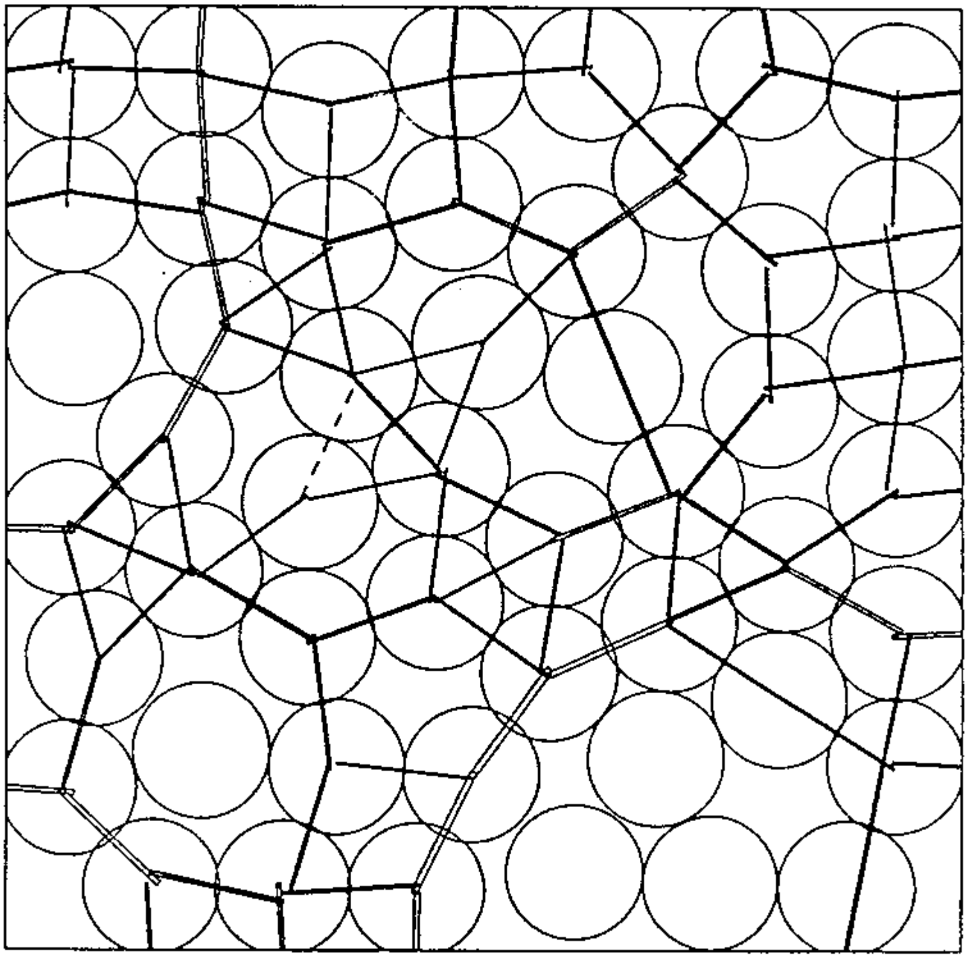

Figure 3.11. Initial condition (C = 0.8)

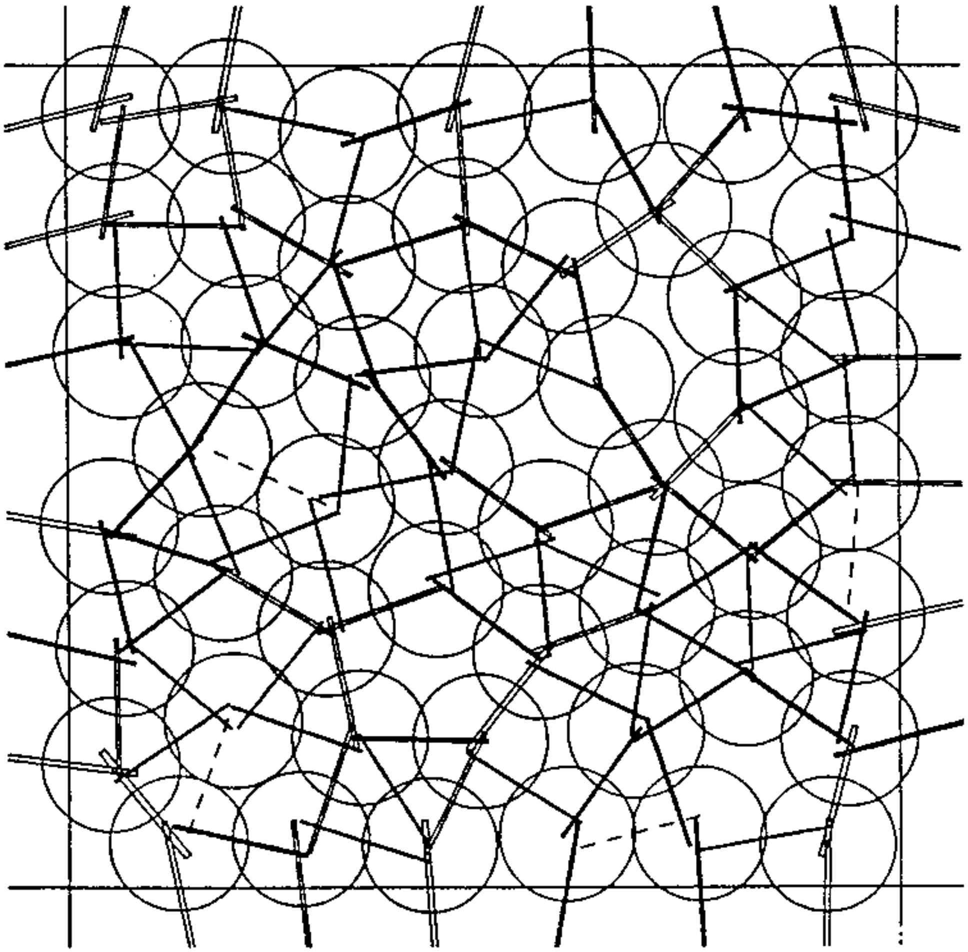

Figure 3.12. Uniform compression; inward wall velocity = 0.5

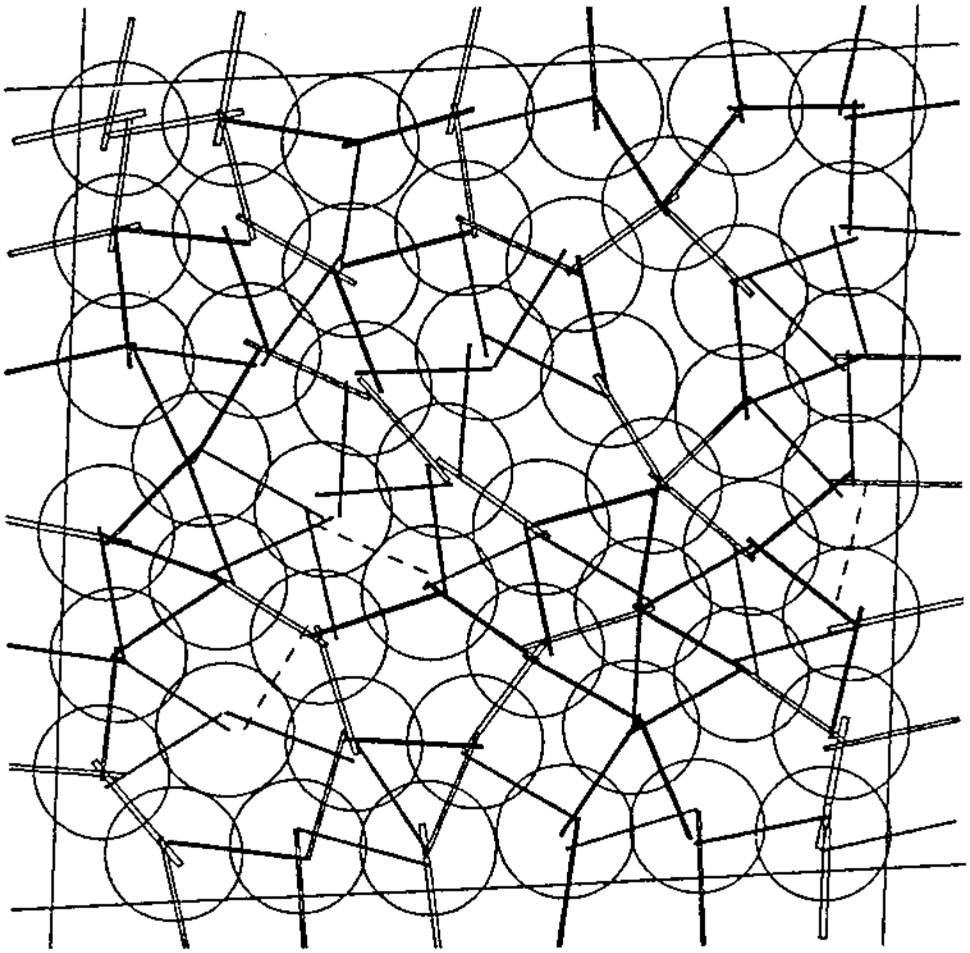

Figure 3.13. Distortion; wall rotation =0.1

3.5 Couette Flow

In this section, the results of Couette flow simulation are presented. The "uniform rectilinear flow" version of the model was used. In this version the streamwise periodic boundary condition is incorporated.

The results of one numerical run are presented as an example. The channel is 10 particle diameters wide (diameter d=1). Walls are roughened by placing semiparticles along the wall. Spacing of boundary particles is specified as zero. Input concentration is C=0.6. From these parameters, program automatically calculated the width of calculation cell (a=3d), number of boundary particles ($N_b = 3$) and number of interior particles ($N = 23$).

The initial condition is automatically generated in two steps (Figure 3.14). First, the pre-initial loose packing is created; and second, this packing was mechanically compressed to obtain desired initial concentration. Finally, particles are assigned random initial velocities to improve speed of simulation (simulation is controlled by collision counter).

The Couette flow situation is then created by pulling walls in opposite directions with velocity $U_o = 10$. One typical instant of simulation is illustrated in Figure 3.15, where configuration, forces and velocities of particles are shown.

Statistical averages are taken between specified number of collissions per particle. Collisions occurring in the flow are counted as broken contacts. The results are presented in form of the mean concentration and mean velocity profiles for three averaging periods (500-1000, 1000-1500 and 1500-2000 collisions per particle). These profiles are shown in Figure 3.16. It appears from the figure that flow has approximately reached steady state, although this is difficult to confirm.

The parameters used for this run are listed in the following page.

```
Couette Flow Simulation
************************

material parameters:
particle radius        R=    0.50
particle density    dens=    1.00
normal stiffness     akn=10000.00
shear stiffness      aks=10000.00
restitution coef.    eps=  0.8000
normal damping coef.  zn=  0.0709
shear damping coef.   zs=  0.0708
friction coefficient amu=  0.2679

time step dt=   0.00279

problem specification:
average concentration  c=  0.60
channel width          b= 10.00
calculation cell width a=  3.00
boundary particles separation sw=  0.00
number of interior particles               np=   23
number of boundary particles on one wall   nb=    3
total # of particles (including periodic)    =   87

flow driver:
gravitational acceleration         g=  0.00
inclination angle of flow plane     =  0.00
lower wall horizontal velocity    u1= 10.00
upper wall horizontal velocity    u2=-10.00

initial condition parameters:
concentration of pre-initial random pack c0=  0.40
number of time steps for "squeezing"   ntsq=  1000
maximum initial fluctuation velocity    vpr=  1.00

statistics limits:
number of time-averaging intervals =  3
  1. average from  500 to 1000 collisions per particle
  2. average from 1000 to 1500 collisions per particle
  3. average from 1500 to 2000 collisions per particle
```

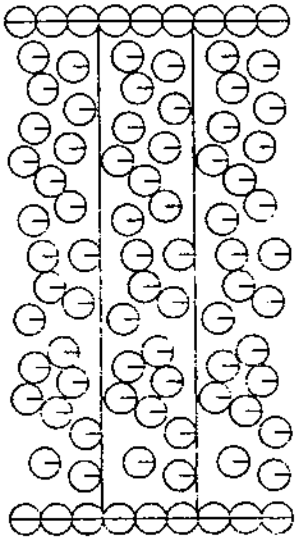

a] pre-initial loose packing

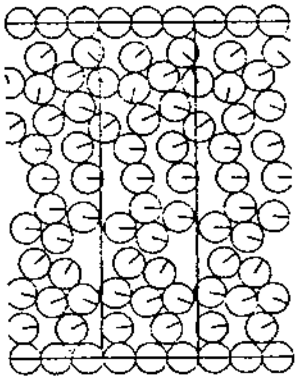

b] initial condition after "squeezing"

Figure 3.14. Generation of initial conditions for Couette flow

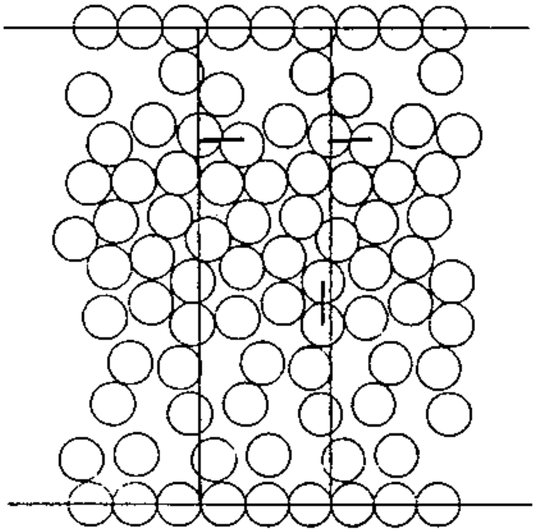

a] force plot

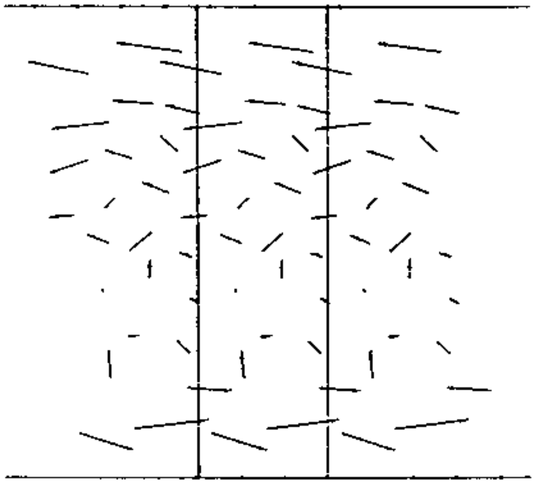

b] velocity plot

Figure 3.15. Characteristic instant of Couette flow simulation

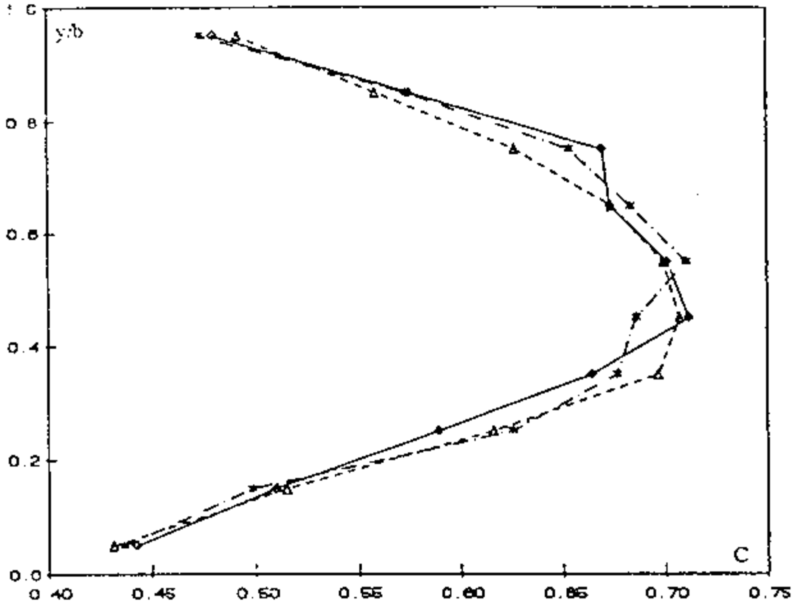

a] mean concentration profile

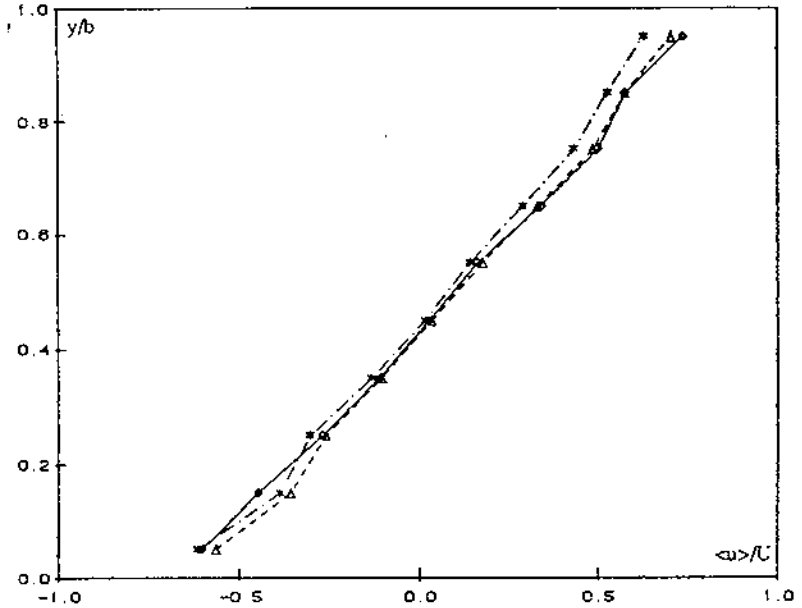

b] mean velocity profile

Figure 3.16. Couette flow, data sets from averaging between 500-1000, 1000-1500, 1500-2000 collisions per particle

3.6 Channel Flow

In this section, the results of gravity driven channel flow simulation are presented. The "uniform rectilinear flow" version of the model with periodic streamwise boundary condition was used.

The parameters used for this run correspond to air-table experiments of Sanders and Ackermann (1986). Particles are uniform circular disks with diameter d=1.75 in (0.0444 m), thickness th=0.25 in (0.00635 m), density $\rho_s = 1121.60$ kg/m^3. The coefficient of restitution is estimated to be $\epsilon \approx 0.95$, and the coefficient of friction $\mu \approx 0.12$. The particle stiffness was selected to be $k_n = 1.E{+}05$ N/m, mainly guided by intention to keep the time step such that simulation can be completed in less than one million time steps. The ratio $k_s/k_n = 0.8$, and shear damping coefficient $\zeta_s = 0$.

For this particular run, the channel is 14 particles wide (b=14d) and the overall concentration C=0.75. The inclination angle of flow plane is $\alpha_o = 0.6^o$. The walls are roughened by placing semiparticles along the wall. The separation of wall particles is specified as zero. The width of periodic cell is calculated by the program as a=5d, and the number of particles in periodic cell as N=67.

The initial conditions were generated in the same way as already described for Couette flow. The gravity is then turned on, and the uniform flow (enforced by periodic boundary condition) developed. The simulation proceeded 50 seconds. The average concentration and velocity profiles were calculated between specified times. The profiles obtained in successive intervals were compared in order to establish steady state condition. It appears that nearly steady state developed after about 15 s.

Figure 3.17. shows configuration and velocity plots at times t=7 s, t=10 s and t=15 s. The development of plug flow in the middle of the channel can be observed. It appears from figures that the plug was already developed at t=10 s. The particles in the plug are in dense hexagonal packing, with nearly uniform velocities. The plug

seems to be 7-9 layers wide. Sanders and Ackermann have also observed the plug formation in 14 diameters wide channel. The closer look at the plug can be taken with the aid of force plot, shown in Figure 3.18. This plot shows instantaneous system configuration and forces at t=20 s. It can be seen from figure that particles in the plug are not "interlocked", i.e. in continuous contacts. Many particles that are close by are not actually in contact. These particles that are in the contact are in fact undergoing short "collisions" that can be multiple (i.e. particle can be in simultaneous contact with more than one neighbor at the time).

The development of mean velocity profile in time is shown in Figure 3.19. Dashed lines correspond to averaging between 1-4 s, 4-7 s, 7-10 s, 10-15 s in increasing sense. Symbol points correspond to averaging between 15-20 s, 20-25 s, 25-30 s, 30-35 s, 35-40 s, 40-45 s, and 45-50 s. The velocities are no longer increasing, but rather oscillating about apparent steady state. The solid line in Figure 3.19. correspond to average between 15-50 s (steady state mean velocity profile).

Maximum mean velocity (at the middle of the channel) is plotted versus time in Figure 3.20. The oscillatory approach to steady state is an interesting feature which can be clearly seen on this figure. The dashed line correspond to average value from 15-50 s, which is u=0.708 m/s. The mean concentration profile (15-50 s) is shown in Figure 3.21, and the mean transversal velocity profile is shown in Figure 3.22. The concentration profile is slightly asymetric, and transversal velocities are not exactly zero. This is believed to be associated with oscillations in longitudinal velocities. All of these features are expected to stabilize in subsequent times, since oscillations will be damped by energy dissipation mechanisms.

```
Channel Flow Simulation
***********************


material parameters:
particle radius          R=    0.0222  m
particle thickness   thic=     0.00635 m
particle density     dens=     1121.60 kg/m3
normal stiffness      akn=    0.10E+06 N/m
shear stiffness       aks=    0.80E+05 N/m
restitution coef.     eps=    0.9500
normal damping coef.   zn=    0.0163
shear damping coef.    zs=    0.0000
friction coefficient amu=     0.1200

time step dt=   0.00010 s

problem specification:
average concentration   c=  0.75
channel width           b=  0.62 m
calculation cell width a=   0.22 m
boundary particles separation sw=  0.00
number of interior particles                    np=   67
number of boundary particles on one wall      nb=     5
total # of particles (including periodic)        =  231

flow driver:
gravitational acceleration          g=  9.81 m/s2
inclination angle of flow plane      =  0.60 deg
lower wall horizontal velocity     u1=  0.00 m/s
upper wall horizontal velocity     u2=  0.00 m/s

initial condition parameters:
concentration of pre-initial random pack c0=  0.40
number of time steps for "squeezing"   ntsq=  1000
maximum initial fluctuation velocity     vpr=  0.10 m/s

statistics limits:
number of time-averaging intervals = 11

  1. average from  10000 to  40000 time steps
  2. average from  40000 to  70000 time steps
  3. average from  70000 to 100000 time steps
  4. average from 100000 to 150000 time steps
  5. average from 150000 to 200000 time steps
  6. average from 200000 to 250000 time steps
  7. average from 250000 to 300000 time steps
  8. average from 300000 to 350000 time steps
  9. average from 350000 to 400000 time steps
 10. average from 400000 to 450000 time steps
 11. average from 450000 to 500000 time steps
```

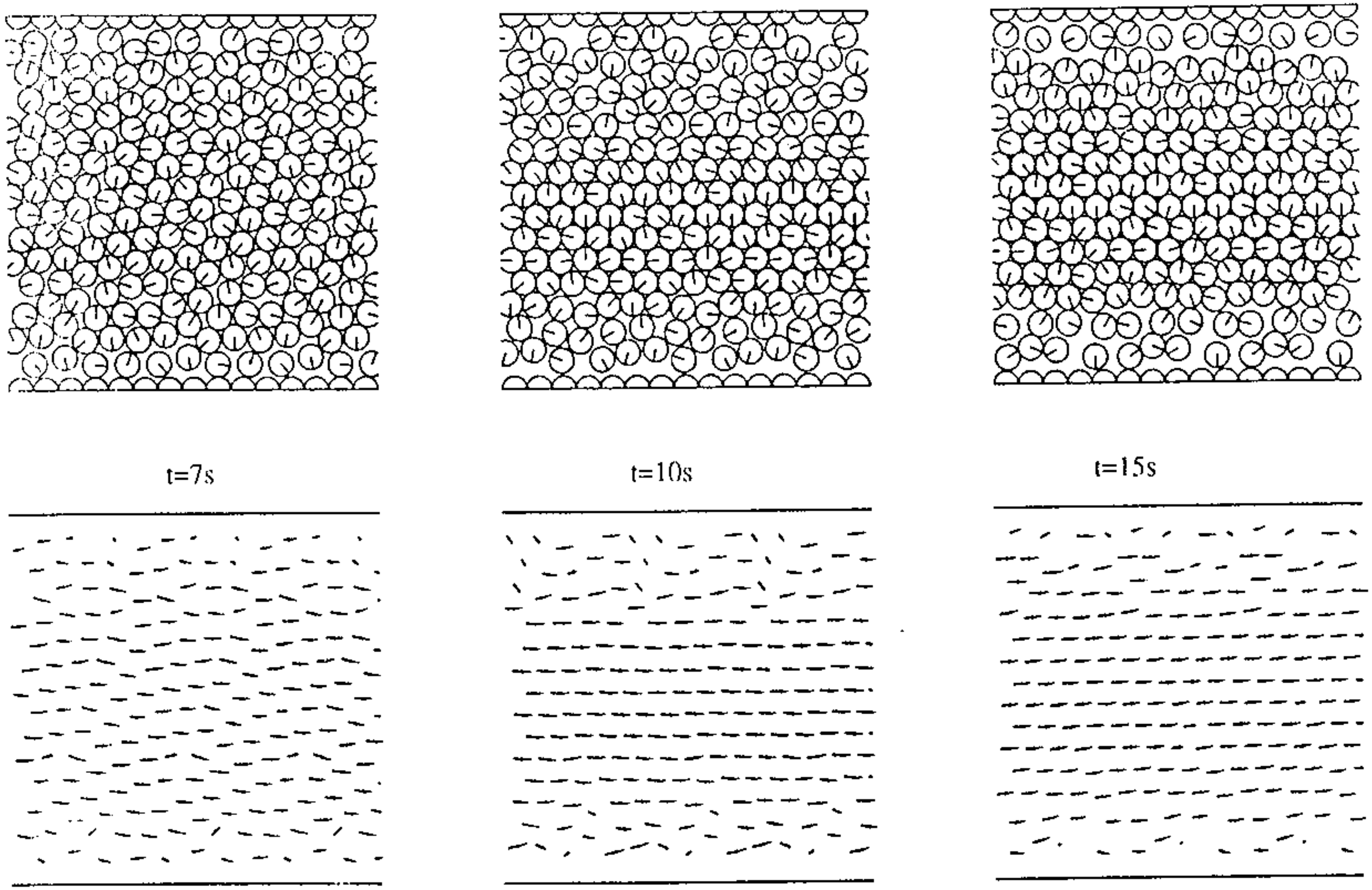

Figure 3.17. Simulation of the gravity-driven channel flow. Note the plug formation.
Top sequence shows configuration plots, bottom sequence shows velocity plots.
(velocities are scaled by maximum instantaneous velocity)

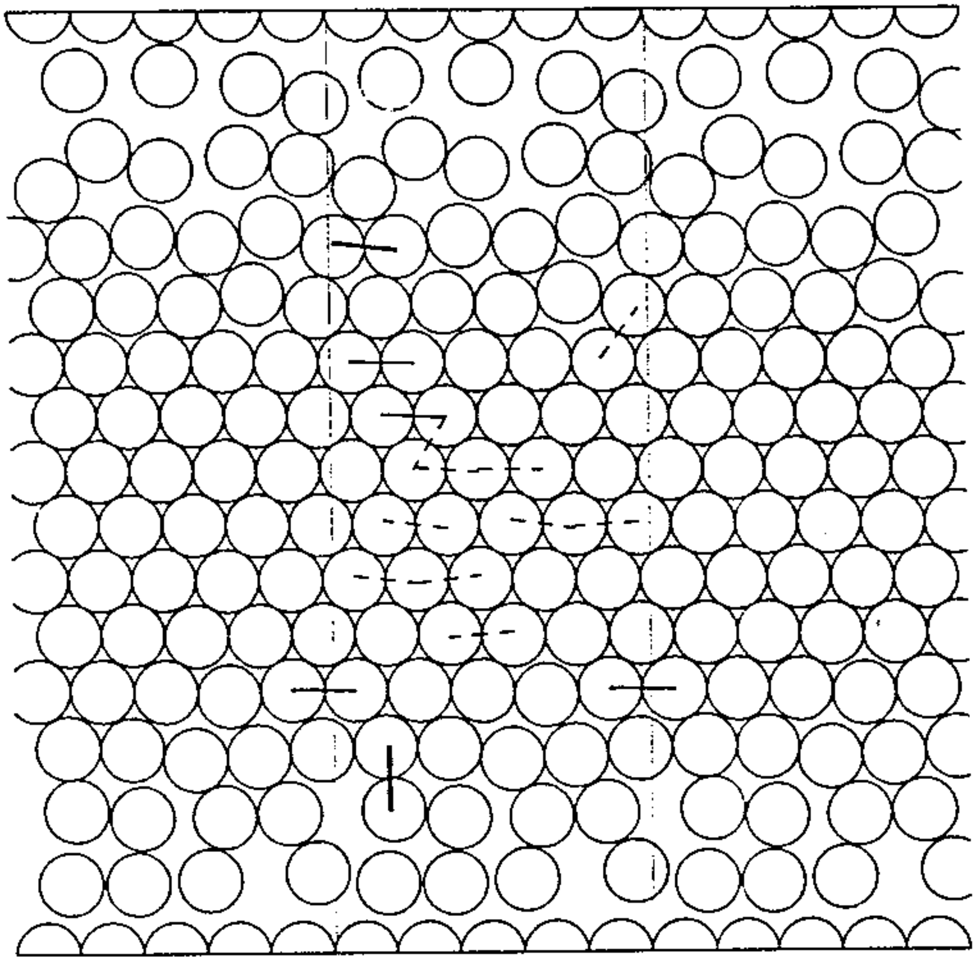

Figure 3.18. Channel flow force plot, t=20s.

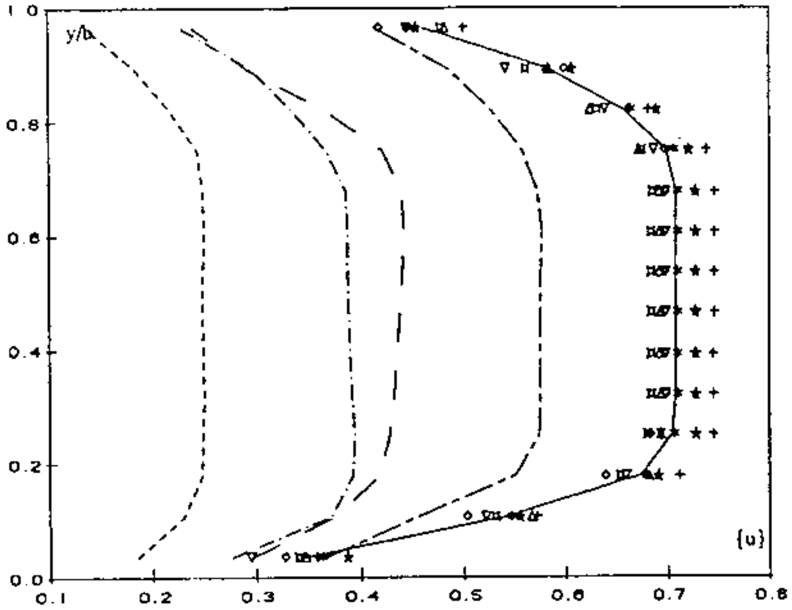

Figure 3.19. Mean velocity profiles in channel flow

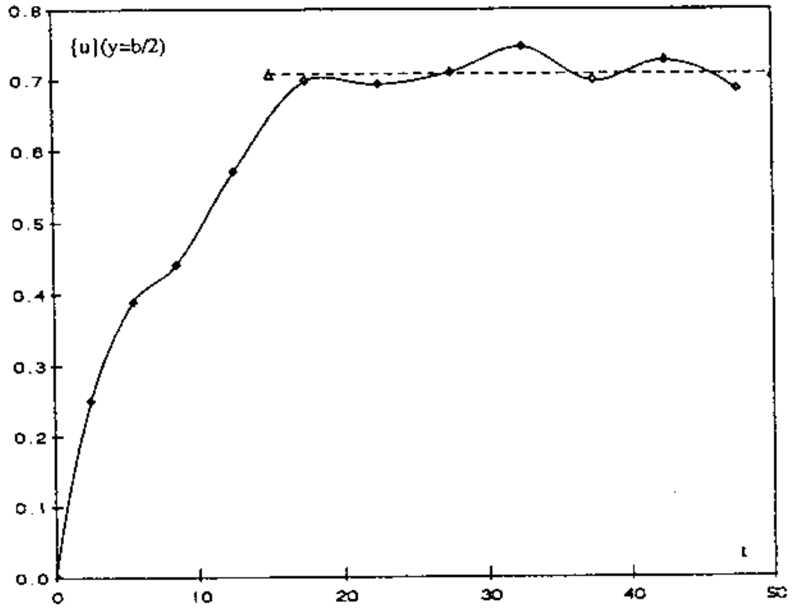

Figure 3.20. Development of maximum mean velocity in time

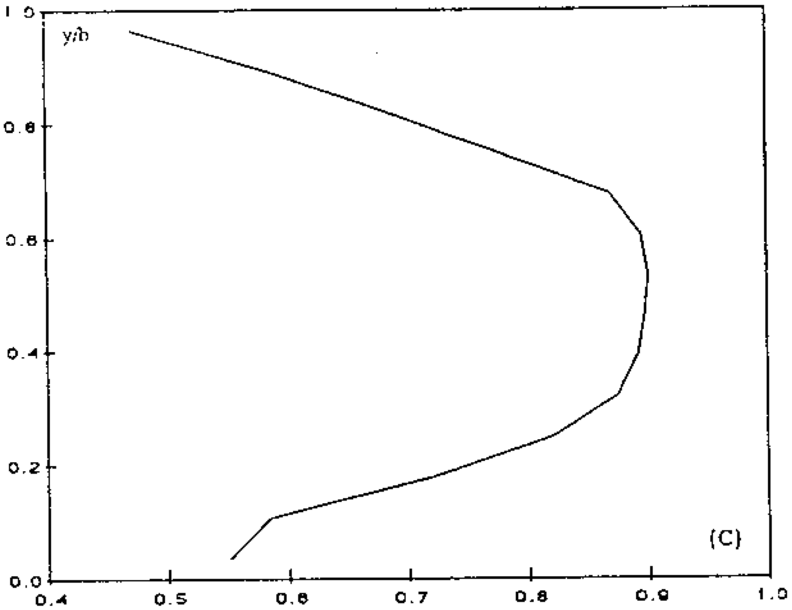

Figure 3.21. Mean concentration profile in channel flow

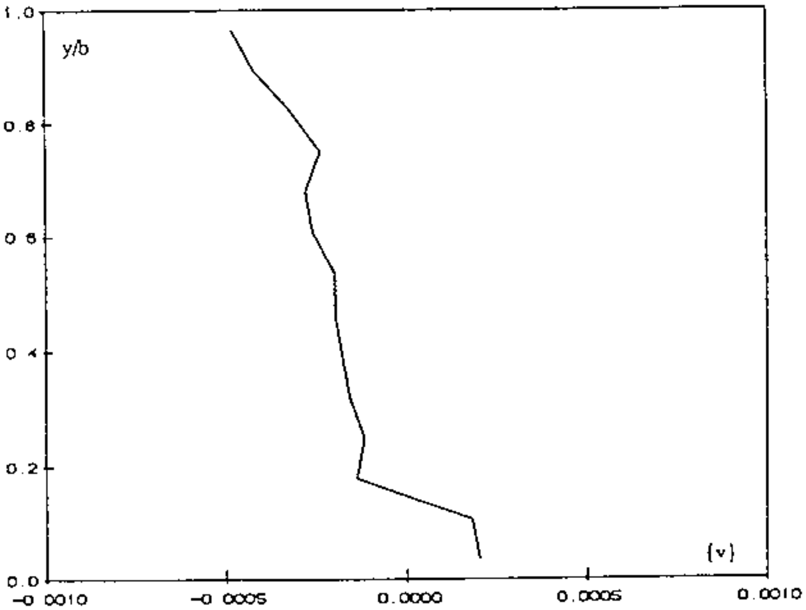

Figure 3.22. Mean transversal velocity profile in channel flow

From the results of this run, some predictions can be made for the case of ice flow on the basis of dimensional scaling. The relevant dynamical time scale of the process is $T = \sqrt{d/g_x}$, and velocity scale is $U = \sqrt{g_x d}$. In this run, $T \approx 0.65$ s and $U \approx 0.0067$ m/s. The approach to steady state takes about $30T$, and maximum velocity (at steady state) is about $10U$.

Keeping the geometrical similarity (b=10d) and concentration (C=0.75) the same, and using d=1m, $\alpha_o = 0.00005$, for typical ice flow on the water surface (neglecting current effect) one obtains $T = 45.15$ s and $U = 0.0222$ m/s. Thus, the approach to steady state would take $30T \approx 1300$ s and steady state velocity would be $10U \approx 0.2$m/s. The profiles are expected to be similar because of geometrical similarity. However, the direct simulation and confirmation of this argument would require much longer computation which is at this preliminary stage unnecessary.

Chapter 4

Conclusions

4.1 Summary

In this report, a numerical model for dynamical simulation of granular material behavior and its preliminary applications are described. The model is based on the soft-particle approach, which is applicable to both quasi-static and dynamic problems.

Several versions of the model have been developed. These include the general system (intended to be used for the problems with complex geometry), rectangular wall bounded system (intended to be used for the quasi-static problems) and uniform rectilinear flow (channel, Couette or chute flow).

The preliminary results of the model include the nine-disc verification test, two illustrative examples of general flows (discharge from the bin and flow down the cascade of chutes), the slow deformation of material in rectangular wall bounded system and profiles of concentration and velocity in Couette and channel flows.

These preliminary results are in all respects satisfactory, and demonstrate validity and capabilities of the present model.

4.2 Future Work

Present model is intended to be used to provide guidance for theoretical efforts to derive general constitutive equations for granular flow, including quasi-static, transitional and rapid flow regimes. The particular application of such a complete granular flow theory is the problem of dynamic transport of river ice and ice jams. By coupling the ice-transport equations with the fluid flow equations of the river, a mathematical model can be developed for ice transport and jam initiation in rivers.

In this respect, the simple shear flow version of the model will be developed first. In the simple shear flow the mean velocity gradient, concentration and mechanical temperature are constant everywhere in the flow field. In the numerical model, this flow is simulated using periodic boundary conditions in all directions. The detailed parametric study will be performed, focusing the attention particularly on the transition and quasi-static regimes that are not well understood.

In addition, the numerical experiments (direct simulation) of the ice-related phenomena can be devised. The gravity driven flow of ice particles in a channel can be studied, including effects of different forces acting on ice particles such as water drag on the bottom surface, form drag on the perimeter of the particle, wind shear on the top surface etc. Ice jam formation can be investigated by imposing appropriate boundary conditions and channel geometry (curvature, contraction, change of slope, obstacles etc.).

Present model can be further extended to the case of nonuniformly sized particles and nonuniformly shaped particles fairly easily, and these extensions will be made if necessary.

References

1. Campbell, C. S. (1982). "Shear flows of granular materials", Ph.D. Dissertation, California Institute of Technology, Pasadena, California.
2. Campbell, C. S. and Brennen, C. E. (1985a). "Computer simulation of granular shear flows", *J. Fluid Mech.*, 151, 167-188.
3. Campbell, C. S. and Brennen, C. E. (1985b). "Chute flows of granular materials: some computer simulations", *J. Appl. Mech*, 52, 172-178.
4. Campbell, C. S. and Gong, A. (1986). "The stress tensor in a two-dimensional granular shear flow", *J. Fluid Mech.* ,164, 107-125.
5. Cundall, P. A. and Strack, O. D. L. (1979a). "A discrete numerical model for granular assemblies", *Geotechnique*, 29, 47-65.
6. Cundall, P. A. and Strack, O. D. L. (1979b). "The distinct element method as a tool for research in granular media", Report to NSF, Parts I and II, Dept. Civ. Min. Engng. Univ. Minnesota
7. Cundall, P.A., Drescher, A. and Strack, O. D. L. (1982). "Numerical experiments in granular assemblies: measurements and observations", in *Deformation and failure of granular materials* 255-270. Eds P.A. Vermeer and H.J. Luger, Balkema, Rotterdam.

8. Cundall, P. A. and Strack, O. D. L. (1983). "Modeling of microscopic mechanisms in granular material", in *Mechanics of granular materials: new models and constitutive relations*, J.T. Jenkins and M. Satake, eds., Elsevier Sci. Pub.

9. Haff, P. K. (1987). "Micromechanical aspects of sound waves in granular material", in Brown Bag Preprint Series in Basic and Applied Science, BB-66.

10. Hopkins, M. A. (1985). "Collisional stresses in a rapidly deforming granular flows", M.S. Thesis, Clarkson University, Potsdam, N.Y.

11. Hopkins, M. A. and Shen, H. H. (1988). "A Monte Carlo simulation of a simple shear flow of granular materials", in *Micromechanics of granular materials* M. Satake and J. T. Jenkins eds., Elsevier Sci. Pub.

12. Hopkins, M. A. (1987). "Particle Simulation: Volume I", Report No. 87-7, Dept. of Civil and Environmental Engng., Clarkson University, Potsdam, N.Y.

13. Sanders, B.E. and Ackermann, N.L. (1986). "Two-dimensional gravity driven granular flow: experimental data", *Society of Engng. Sciences 23. Ann. Tech. Meeting, State University, Buffalo, New York, August 25-27,1986*, preprint ESP23.86045.

14. Thornton, C. and Barnes, D. J. (1986). "Computer simulated deformation of compact granular assemblies", *Acta Mechanica*, 64, 45-61.

15. Walton, O. R. (1983). "Explicit particle dynamics model for granular materials", in *Numerical methods in geomechanics*, Z. Eisenstein, ed. A. A. Balkema, Rotterdam, 1261-1268.

16. Walton, O. R. (1983). "Particle-dynamics calculations of shear flows" in *Mechanics of granular materials: new models and constitutive relations*, J.T. Jenkins and M. Satake, eds., Elsevier Sci. Pub.

17. Walton, O. R. and Braun, R. L. (1985). "Viscosity, granular temperature and stress calculations for shearing assemblies of inelastic, frictional disks", *J. Rheol.*, 30, 949-980.

18. Walton, O. R. and Braun, R. L. "Stress calculations for assemblies of inelastic spheres in uniform shear", *Acta Mech.* (To appear).

19. Werner, B. T. and Haff, P. K. (1986). "Dynamical simulation of granular material using concurrent processing computers", *Geotechnique* (To appear).

Appendix A

Binary Contact Mechanics

In this section the mechanics of binary contact (collision) using the contact force model described in section 2.3.2. is analyzed in detail. The purpose of this analysis is to establish analytical equations governing time evolution of both normal and tangential displacements and forces. On the basis of analytical solution for normal impact, analytical expressions for relationship between contact damping and coefficient of restitution as well as for duration of binary contact (critical time step) are derived. Furthermore, for the comparison with rigid body models, the effective coefficient of rotational restitution β is determined as a function of soft particle properties.

Consider the binary contact of identical disks 1 and 2 shown in Figure A.1. The origin of Cartesian coordinate system (x,y,z) is taken to be at the point of contact at time $t = 0$. The position vectors of centers of disks 1 and 2 with respect to this origin are represented as $\mathbf{r}_1$ and $\mathbf{r}_2$, respectively. The velocity vectors of centers of disks 1 and 2 are represented as $\dot{\mathbf{r}}_1$ and $\dot{\mathbf{r}}_2$, and the angular velocities are $\dot{\theta}_1$ and $\dot{\theta}_2$, taken as positive in counterclockwise direction.

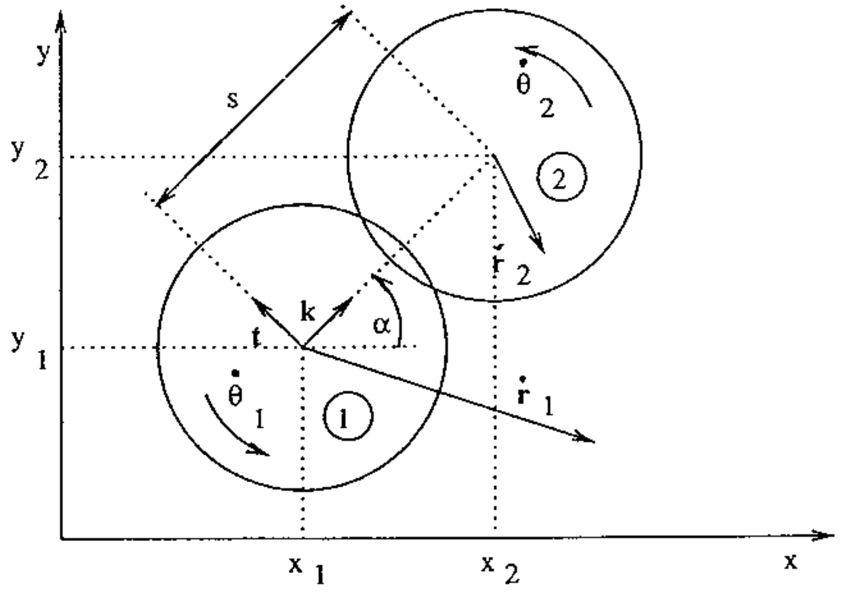

Figure A.1. Contact between two particles

The equations of motion will be expressed in a new coordinate system (k,t,z) defined by the unit vector k pointing from the center of disc 1 to the center of disc 2 and the unit vector t obtained by a counterclockwise rotation of k through 90°, i.e.

$$\mathrm{k} = \frac{\mathbf{r}_2 - \mathbf{r}_1}{|\mathbf{r}_2 - \mathbf{r}_1|} = (\cos\alpha, \sin\alpha); \qquad \mathbf{t} = (-\sin\alpha, \cos\alpha) \tag{A.1}$$

The time derivatives of unit vectors $\mathbf{k}$ and $\mathbf{t}$ are in general not equal to zero, because of rotations of particles. They can be expressed as

$$\dot{\mathbf{k}} = \dot{\alpha}(-\sin\alpha, \cos\alpha) = \dot{\alpha}\mathbf{t}; \qquad \dot{\mathbf{t}} = \dot{\alpha}(-\cos\alpha, -\sin\alpha) = -\dot{\alpha}\mathbf{k} \tag{A.2}$$

Term $\dot{\alpha}$ is actually the rate of rotation of coordinate system (k, t) about the center of mass (which is in this case equivalent to contact point), and can be found from kinematics of rotation to be

$$\dot{\alpha} = \dot{\theta}_1 + \dot{\theta}_2 \tag{A.3}$$

The equations of linear motion (Newton's second law) for disks 1 and 2 are given by

$$m\ddot{\mathbf{r}}_1 = \mathbf{F}_{12} \tag{A.4}$$

$$m\ddot{\mathbf{r}}_2 = \mathbf{F}_{21} \tag{A.5}$$

where $\mathbf{F}_{12}$ is the contact force acting on disk 1 from disk 2 and $\mathbf{F}_{21} = -\mathbf{F}_{12}$ is the contact force acting on disk 2 from disk 1. Adding these equations, one obtains the equation of motion $\ddot{\mathbf{R}} = 0$ for the center of mass $\mathbf{R} = \frac{1}{2}(\mathbf{r}_1 + \mathbf{r}_2)$. This equation expresses the principle of conservation of linear momentum $\dot{\mathbf{R}} = \dot{\mathbf{R}}_o = \text{const}$.

Subtracting equations (A.4) and (A.5), one obtains the equation of motion for the relative position $\mathbf{r} = \mathbf{r}_1 - \mathbf{r}_2$

$$m\ddot{\mathbf{r}} = \mathbf{F} \tag{A.6}$$

where $\mathbf{F} = 2\mathbf{F}_{12}$.

The total contact force $\mathbf{F}_{12}$ on disc 1 can be decomposed into normal and tangential component as follows

$$\mathbf{F}_{12} = -\left((F_n + D_n)\mathbf{k} + (F_s + D_s)\mathbf{t}\right) \tag{A.7}$$

By the sign convention, F_n and D_n are taken to be positive in $-\mathbf{k}$ direction and F_s and D_s are taken to be positive in $-\mathbf{t}$ direction.

The governing vector equation for the relative position $\mathbf{r} = \mathbf{r}_1 - \mathbf{r}_2$ is given by (A.6). Taking the components of this equation in $\mathbf{k}$ and $\mathbf{t}$ direction and using (A.7) yields two scalar equations:

$$m\ddot{\mathbf{r}} \cdot \mathbf{k} + 2(F_n + D_n) = 0 \tag{A.8}$$

$$m\ddot{\mathbf{r}} \cdot \mathbf{t} + 2(F_s + D_s) = 0 \tag{A.9}$$

Components of $\dot{\mathbf{r}}$ in normal and tangential direction are

$$\dot{n} = \dot{\mathbf{r}} \cdot \mathbf{k} \tag{A.10}$$

$$\dot{s} = \dot{\mathbf{r}} \cdot \mathbf{t} \tag{A.11}$$

The relative displacements in normal and tangential direction n and s are:

$$n = \int_0^t \dot{n}dt; \qquad s = \int_0^t \dot{s}dt \tag{A.12}$$

The relative velocity at the contact point $\mathbf{g}_{12}$ is given by

$$\mathbf{g}_{12} = \dot{\mathbf{r}}_1 - \dot{\mathbf{r}}_2 + R(\dot{\theta}_1 + \dot{\theta}_2)\mathbf{t} = \dot{\mathbf{r}} + R\dot{\alpha}\mathbf{t} \tag{A.13}$$

The components of $\mathbf{g}_{12}$ in normal and tangential directions are

$$\mathbf{g}_{12} \cdot \mathbf{k} = \dot{\mathbf{r}} \cdot \mathbf{k} = \dot{n} \tag{A.14}$$

$$\mathbf{g}_{12} \cdot \mathbf{t} = \dot{\mathbf{r}} \cdot \mathbf{t} + R\dot{\alpha} = \dot{s} + R\dot{\alpha} \equiv \dot{q} \tag{A.15}$$

In order to express equations (A.8) and (A.9) in terms of n and s, by taking time derivative of equations (A.10) and (A.11) one obtains:

$$\ddot{\mathbf{r}} \cdot \mathbf{k} = \ddot{n} - \dot{\mathbf{r}} \cdot \dot{\mathbf{k}} = \ddot{n} - \dot{\alpha}\dot{\mathbf{r}} \cdot \mathbf{t} = \ddot{n} - \dot{s}\dot{\alpha} \tag{A.16}$$

$$\ddot{\mathbf{r}} \cdot \mathbf{t} = \ddot{s} - \dot{\mathbf{r}} \cdot \dot{\mathbf{t}} = \ddot{s} + \dot{\alpha}\dot{\mathbf{r}} \cdot \mathbf{k} = \ddot{s} + \dot{n}\dot{\alpha} \tag{A.17}$$

These results can now be assembled and substituted into equations (A.8) and (A.9) to yield

$$\ddot{n} - \dot{s}\dot{\alpha} + \frac{2}{m}(F_n + D_n) = 0 \tag{A.18}$$

$$\ddot{s} + \dot{n}\dot{\alpha} + \frac{2}{m}(F_s + D_s) = 0 \tag{A.19}$$

The equation governing the evolution of α can be obtained from the equations of angular motion for disks 1 and 2, which are given by

$$I\ddot{\theta}_1 + (\mathbf{r}_1 \times \mathbf{F}_{12})_z = 0 \tag{A.20}$$

$$I\ddot{\theta}_2 + (\mathbf{r}_2 \times \mathbf{F}_{21})_z = 0 \tag{A.21}$$

Adding these equations, using (A.3) and (A.7) and $\mathbf{r} \cdot \mathbf{t} = 0$, one obtains

$$\ddot{\alpha} = -\frac{1}{I}(\mathbf{r} \times \mathbf{F}_{12})_z = \frac{1}{I}(F_s + D_s)(\mathbf{r} \cdot \mathbf{k}) \tag{A.22}$$

But,

$$\mathbf{r} \cdot \mathbf{k} = (\mathbf{r} \cdot \mathbf{k})_0 + \int_0^t (\mathbf{r} \dot{\cdot} \mathbf{k})dt = -2R + \int_0^t ((\dot{\mathbf{r}} \cdot \mathbf{k}) + (\mathbf{r} \cdot \dot{\mathbf{k}}))dt =$$

$$= -2R + \int_0^t ((\dot{\mathbf{r}} \cdot \mathbf{k}) + \dot{\alpha}(\mathbf{r} \cdot \mathbf{t}))dt = -2R + \int_0^t \dot{n}dt = -2R + n \tag{A.23}$$

Hence,

$$\ddot{\alpha} = -\frac{2R - n}{I}(F_s + D_s) \tag{A.24}$$

System of equations (A.18), (A.19), and (A.24) now determines the motion of the system in terms of contact force components. It remains to specify the force-displacement law to close this system of equations which can then be solved for specified initial conditions. The normal force is given by

$$F_n + D_n = K_n n + C_n \dot{n} \tag{A.25}$$

The tangential force is given in conditional incremental form as

$$(F_s + D_s)^N = (F_s + D_s)^{N-1} + K_s \dot{q} \Delta t + C_s \dot{q} \tag{A.26}$$

or,

$$\text{if} \quad |F_s^{N-1} + K_s \dot{q} \Delta t| > F_n^{N-1} + \mu K_n \dot{n} \Delta t$$

$$(F_s + D_s)^N = \Lambda \mu K_n n; \qquad \Lambda = sign(F_s^{N-1} + K_s \dot{q} \Delta t) \tag{A.27}$$

The superscripts N and N-1 denote times t_N and t_{N-1}, such that $\Delta t = t_N - t_{N-1}$. In the above equations K_n and K_s are normal and tangential effective contact stiffnesses, C_n and C_s are contact damping coefficients and μ is the coefficient of friction. The effective stiffnesses (springs connected in series) are given in terms of particle stiffnesses k_n and k_s as $K_n = k_n/2$ and $K_s = k_s/2$.

Substituting equations (A.25) and (A.26) into (A.18), (A.19), and (A.24) and rearranging yields

$$\ddot{n} + 2\zeta_n \omega_o \dot{n} + \omega_o^2 n - \dot{s}\dot{\alpha} = 0 \tag{A.28}$$

$$\ddot{s} + \dot{n}\dot{\alpha} + \omega_o^2 S = 0 \tag{A.29}$$

$$\ddot{\alpha} + \omega_o^2 (2 - \frac{n}{R}) \frac{S}{R} = 0 \tag{A.30}$$

where

$$S = \frac{F_s + D_s}{K_n} \tag{A.31}$$

and

$$\omega_o = \sqrt{\frac{k_n}{m}} \tag{A.32}$$

$$\zeta_n = \frac{C_n}{m\omega_o}; \qquad \zeta_s = \frac{C_s}{m\omega_o} \tag{A.33}$$

Here ζ_n and ζ_s are dimensionless damping coefficients in normal and tangential directions, respectively.

The system of 3 nonlinear ordinary differential equations (A.28) (A.29) (A.30) with (A.31) can now be solved for given initial conditions $n(0)$, $s(0)$, $\alpha(0)$, $\dot{n}(0)$, $\dot{s}(0)$ and $\dot{\alpha}(0)$. The initial conditions (pre-collisional quantities) can be defined as

$$\mathbf{r}_1(0) = -R\mathbf{k}_o; \qquad \mathbf{r}_2(0) = R\mathbf{k}_o \tag{A.34}$$

$$\dot{\mathbf{r}}_1(0) = \mathbf{c}_1; \qquad \dot{\mathbf{r}}_2(0) = \mathbf{c}_2 \tag{A.35}$$

$$\theta_1(0) = \omega_1; \qquad \theta_2(0) = \omega_2 \tag{A.36}$$

where $\mathbf{k}_o = (\cos\alpha_o, \sin\alpha_o)$. Therefore, the initial conditions for the system (A.28) (A.29) (A.30) with (A.31) can be written as

$$n(0) = 0; \qquad s(0) = 0; \qquad \alpha(0) = \alpha_o \tag{A.37}$$

$$\dot{n}(0) = (\mathbf{c}_1 - \mathbf{c}_2) \cdot \mathbf{k}_o = c_{12} \cos\gamma_o \equiv c_n^o \tag{A.38}$$

$$\dot{s}(0) = c_{12} \sin\gamma_o \tag{A.39}$$

$$\dot{\alpha}(0) = \omega_1 + \omega_2 \tag{A.40}$$

Also,

$$\dot{q}(0) = \dot{s}(0) + R\dot{\alpha}(0) = c_{12} \sin\gamma_o + R(\omega_1 + \omega_2) \equiv c_s^o \tag{A.41}$$

From the solution components $n(t)$, $s(t)$ and $\alpha(t)$, all other informations can be deduced. The contact force components are given by (A.25) and (A.26). The velocities of disks 1 and 2 can be found as

$$\dot{\mathbf{r}}_1 = \dot{\mathbf{R}} + \frac{1}{2}\dot{\mathbf{r}} = \dot{\mathbf{R}}_o + \frac{1}{2}(\dot{n}\mathbf{k} + (\dot{s} - R\dot{\alpha})\mathbf{t}) \tag{A.42}$$

$$\dot{\mathbf{r}}_2 = \dot{\mathbf{R}} - \frac{1}{2}\dot{\mathbf{r}} = \dot{\mathbf{R}}_o - \frac{1}{2}(\dot{n}\mathbf{k} + (\dot{s} - R\dot{\alpha})\mathbf{t}) \tag{A.43}$$

The positions of centers of disks 1 and 2 can be found as

$$\mathbf{r}_1 = \mathbf{R} + \frac{1}{2}\mathbf{r} = \dot{\mathbf{R}}_{\mathbf{o}}t + \frac{1}{2}(-2R + n)\mathbf{k} \tag{A.44}$$

$$\mathbf{r}_2 = \mathbf{R} - \frac{1}{2}\mathbf{r} = \dot{\mathbf{R}}_{\mathbf{o}}t - \frac{1}{2}(-2R + n)\mathbf{k} \tag{A.45}$$

The x,y components of $\mathbf{r}_1$, $\mathbf{r}_2$, $\dot{\mathbf{r}}_1$ and $\dot{\mathbf{r}}_2$ can be simply obtained using (A.1).

In particular, the post-collisional quantities can be determined from the above equations evaluated at time $t = t_c$, (the moment of separation, when $n(t_c) = 0$). The post-collisional quantities are defined as

$$\mathbf{r}_1(t_c) = -R\mathbf{k}(t_c); \qquad \mathbf{r}_2(t_c) = R\mathbf{k}(t_c) \tag{A.46}$$

$$\dot{\mathbf{r}}_1(t_c) = \mathbf{c}_1^*; \qquad \dot{\mathbf{r}}_2(t_c) = \mathbf{c}_2^* \tag{A.47}$$

$$\theta_1(t_c) = \omega_1^*; \qquad \theta_2(t_c) = \omega_2^* \tag{A.48}$$

The coefficient of restitution ϵ is defined as

$$\epsilon = -\frac{(\mathbf{c}_1^* - \mathbf{c}_2^*) \cdot \mathbf{k}}{(\mathbf{c}_1 - \mathbf{c}_2) \cdot \mathbf{k}} = -\frac{\dot{n}(t_c)}{\dot{n}(0)} = -\frac{c_n^*}{c_n^o} \tag{A.49}$$

The angular coefficient of restitution β (also sometimes called the roughness coefficient) can be defined as

$$\beta = -\frac{(\mathbf{c}_1^* - \mathbf{c}_2^*) \cdot \mathrm{t} + R\dot{\alpha}^*}{(\mathbf{c}_1 - \mathbf{c}_2) \cdot \mathbf{t} + R\dot{\alpha}_o} = -\frac{\dot{q}(t_c)}{\dot{q}(0)} = -\frac{c_s^*}{c_s^o} \tag{A.50}$$

These coefficients are thus implicitly related to the soft particle parameters k_n, k_s, ζ_n, ζ_s and μ through the solution of the problem.

The analytical solution of the equations governing binary contact is in general not possible because of the presence of nonlinear terms associated with tangential force. However, the analytical solution is possible in the particular case of normal impact such that $\gamma_o = 0$ and $\omega_1 = \omega_2 = 0$.

In this case the equations (A.29) and (A.30) are automatically satisfied by trivial solutions $s = 0$, $\alpha = \alpha_o$. Equation (A.28) reduces to

$$\ddot{n} + 2\zeta_n \omega_o \dot{n} + \omega_o^2 n = 0 \tag{A.51}$$

The solution of this linear ODE with $n(0) = 0$ and $\dot{n}(0) = \mathbf{c}_{12} \cdot \mathbf{k} = c_{12} \cos\gamma_o \equiv c_o$ is given by

$$n(t) = \frac{c_o}{\omega_d} e^{-\zeta_n \omega_o t} \sin \omega_d t \tag{A.52}$$

where $\omega_d = \omega_o \sqrt{1 - \zeta_n^2}$. From the above solution, the duration of contact t_c can be found from the condition $n(t_c) = 0$. The result is

$$t_c = \frac{\pi}{\omega_d} \tag{A.53}$$

The dependence of the collision duration t_c on the restitution coefficient is shown in Figure A.3.

The coefficient of restitution can also be deduced from this solution. Since

$$\dot{n}(t_c) = -c_o \exp(-\zeta_n \pi \frac{\omega_o}{\omega_d}) \tag{A.54}$$

and $\dot{n}(0) = c_o$, the equation (A.49) yields

$$\epsilon = \exp(-\pi \frac{\zeta_n}{\sqrt{1 - \zeta_n^2}}) \tag{A.55}$$

Inversion of this relation gives an explicit relationship between normal damping coefficient ζ_n and restitution coefficient ϵ:

$$\zeta_n = \frac{-\ln \epsilon}{\sqrt{\pi^2 + \ln^2 \epsilon}} \tag{A.56}$$

This relationship is plotted in Figure A.2. For the perfectly elastic impact $\epsilon = 1$ and $\zeta_n = 0$ (zero damping) and for the perfectly plastic impact $\epsilon = 0$ and $\zeta_n = 1$ (critical damping).

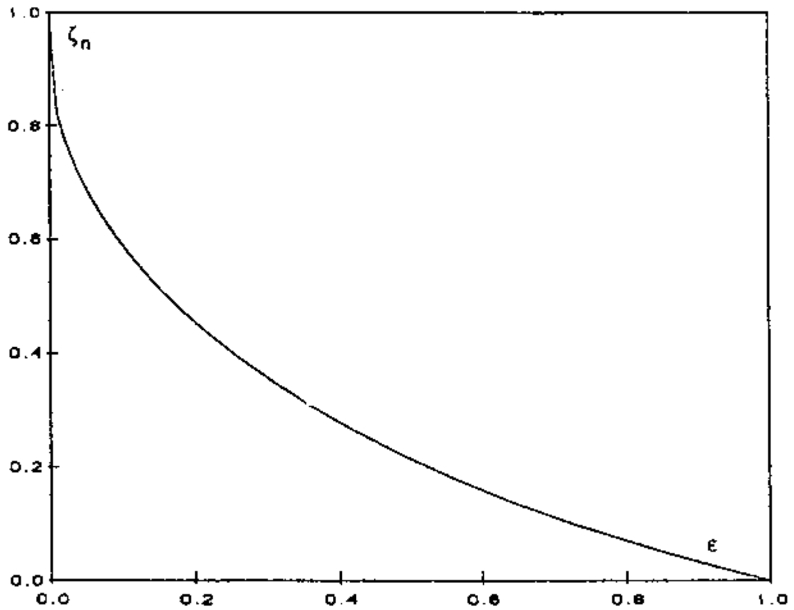

Figure A.2. Relationship between normal damping and restitution coefficients

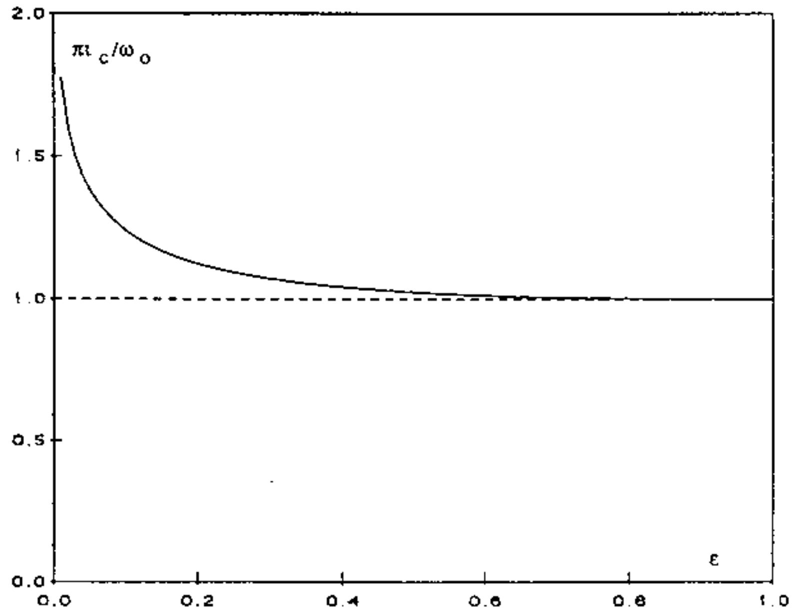

Figure A.3. Dependence of collision duration on restitution coefficient

The numerical solution of system (A.28) (A.29) (A.30) is obtained using the fourth-order Runge-Kutta method. The results are shown in figures A.4-A.7. In these figures time is scaled by collision duration given by equation (A.53), and forces are scaled by $F_m = K_n c_o / \omega_d$.

The normal contact force is shown in Figure A.4, and the normal relative velocity is shown in Figure A.5 for $\epsilon = 0.8$. It is very interesting that the results follow the analytical solution for the normal impact derived above even for oblique impacts (i.e. impact angles $0 < \gamma < \frac{\pi}{2}$). The reason for this is that the nonlinear term in equation (A.16) is negligible compared to inertia and spring terms which are dominant (especially for large values of contact stiffness that have been investigated).

The tangential contact force is shown in Figure A.6, and the tangential relative velocity is shown in Figure A.7 for different impact angles n the range $0 < \gamma < \frac{\pi}{2}$). In thése figures, $\mu = 0.5$, $\epsilon = 0.8$ and $\zeta_s = 0.05$. It can be seen from Figure A.6 that for small impact angles $(5^o, 10^o, 20^o)$ tangential contact force is controlled by tangential spring and dashpot during almost the entire contact. Only at the very end of contact this force exceeds the friction limit, and the contact is sliding from then on until the end. For large impact angles $(70^o, 80^o)$, tangential force is at the friction limit during the entire contact. For intermediate impact angles, tangential force is at the friction limit in the beginning of the contact, then decreases and is governed by spring and dashpot, changes sign and increases until it reaches the friction limit again. The range of impact angles corresponding to these three types of behavior is strongly dependent on the value of friction coefficient μ. For smaller μ values, the contact will be friction-controlled for larger range of impact angles.

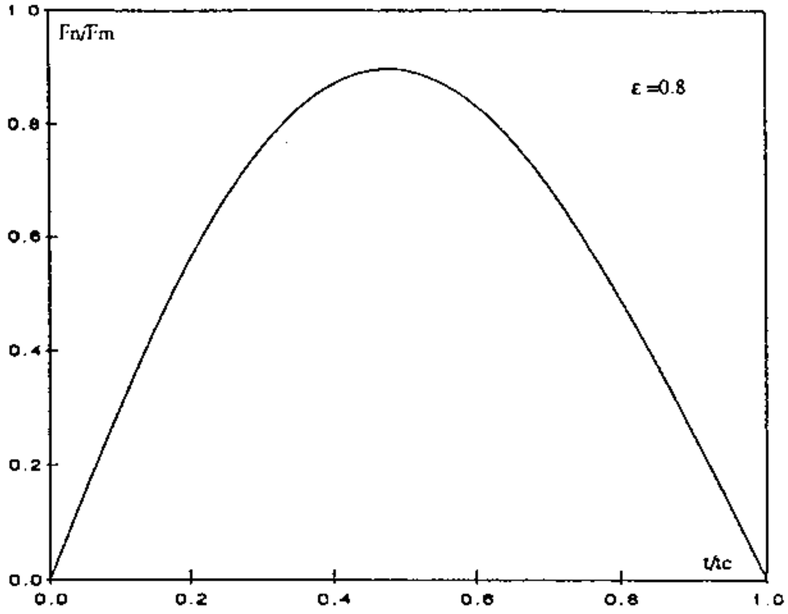

Figure A.4. Development of the normal contact force during a collision

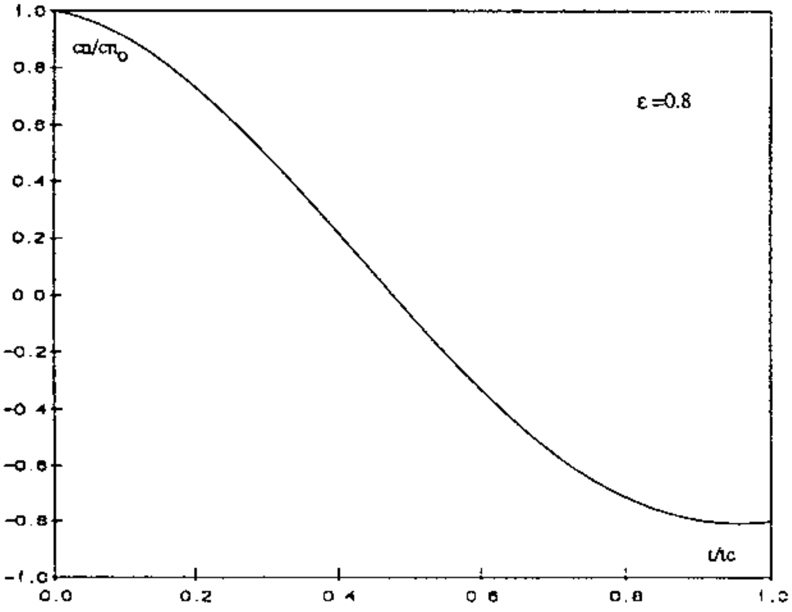

Figure A.5. Development of the normal relative velocity during a collision

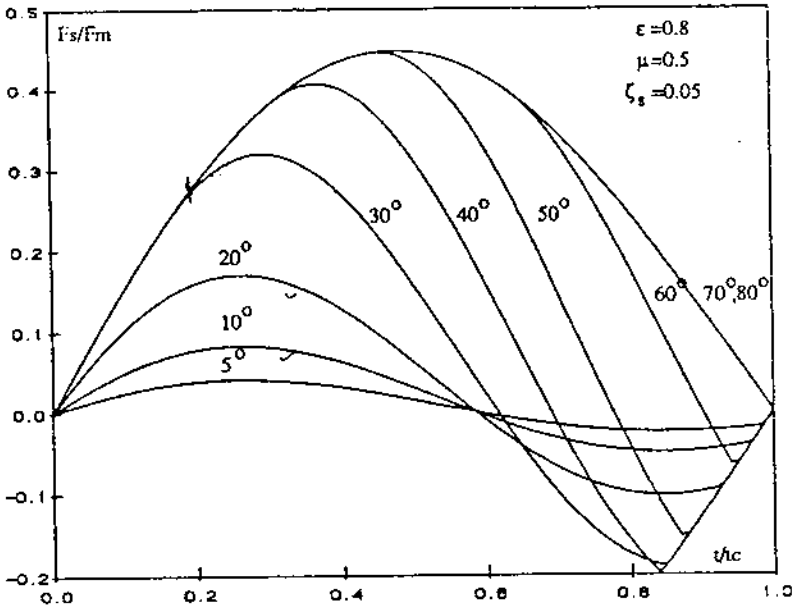

Figure A.6. Development of the tangential contact force during a collision

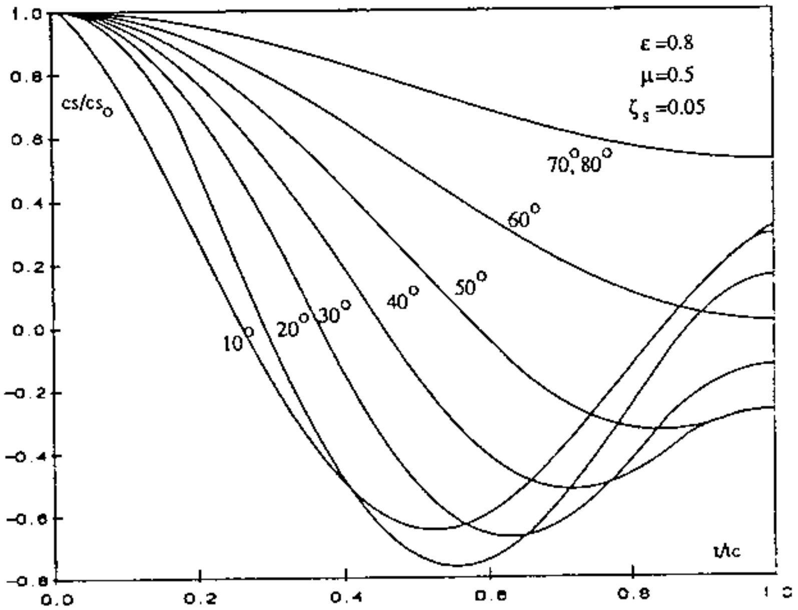

Figure A.7. Development of the tangential relative velocity during a collision

In order to compare present binary contact model with rigid-body collision models, the rigid-body collision equations are reviewed first. The collision equations for the instantaneous rigid-body collision are derived from conservation laws for linear and angular momentum. The conservation of linear momentum can be expressed as

$$m(\mathbf{c}_1^* + \mathbf{c}_2^*) = m(\mathbf{c}_1 + \mathbf{c}_2) \tag{A.57}$$

The conservation of angular momentum about the contact point for disks 1 and 2 can be expressed as

$$I\omega_1^* + \mathbf{r}_1 \times m\mathbf{c}_1^* = I\omega_1 + \mathbf{r}_1 \times m\mathbf{c}_1 \tag{A.58}$$

$$I\omega_2^* + \mathbf{r}_2 \times m\mathbf{c}_2^* = I\omega_2 + \mathbf{r}_2 \times m\mathbf{c}_2 \tag{A.59}$$

In addition, the closure equations for normal and tangential directions are postulated. For the normal direction,

$$(\mathbf{c}_1^* - \mathbf{c}_2^*) \cdot \mathbf{k} = -\epsilon(\mathbf{c}_1 - \mathbf{c}_2) \cdot \mathbf{k} \tag{A.60}$$

The frictional closure equations are of two kinds. If the contact is "sliding" during the entire collision, the tangential force is at the friction limit and therefore the tangential component of the time-integrated force (impulse) is proportional to the normal component of the impulse. The "slip" equation applies, which can be written as

$$(\mathbf{c}_1^* - \mathbf{c}_1) \cdot \mathbf{t} = \mu\Lambda(\mathbf{c}_1^* - \mathbf{c}_1) \cdot \mathbf{k} \tag{A.61}$$

where

$$\Lambda = \mathrm{sign}(\mathbf{g}_{12} \cdot \mathbf{t}) \tag{A.62}$$

Otherwise, the contact is "rolling" and the post-collisional tangential velocity is defined in terms of the angular restitution coefficient β ($-1 \leq \beta \leq 1$) introduced by Lun and Savage (1987). The corresponding "no-slip" equation is given by

$$\mathbf{g}_{12}^* \cdot \mathbf{t} = -\beta(\mathbf{g}_{12} \cdot \mathbf{t}) \tag{A.63}$$

where

$$\mathbf{g}_{12} = \mathbf{c}_1 + \mathbf{r}_1 \times \omega_1 - (\mathbf{c}_2 + \mathbf{r}_2 \times \omega_2) = \mathbf{c}_{12} + R(\omega_1 + \omega_2) \tag{A.64}$$

is the relative precollisional velocity at the point of contact.

For the perfectly smooth particles $\beta = -1$, and the tangential component of relative precollisional velocity is not changed in a collision. For the perfectly rough particles $\beta = 1$ and the tangential component of the relative precollisional velocity is not changed in magnitude but is reversed in direction. In rigid-particle dynamical simulations of Campbell and Brennen (1985) and Hopkins (1987) and Monte Carlo simulation of Hopkins (1986) it was assumed $\beta = 0$. However, it was observed in experiments with plastic and rubber spheres and superballs that spin reversal phenomenon ($0 \leq \beta \leq 1$) did occur, and values of β as high as 0.8 were observed (Lun and Savage (1987)).

Solution of the "no-slip" system (equations (A.57), (A.58), (A.59), (A.60) and (A.63)) is given by

$$\mathbf{c}_1^* - \mathbf{c}_1 = -\frac{1+\epsilon}{2}(\mathbf{c}_{12} \cdot \mathbf{k})\mathbf{k} - \frac{1+\beta}{6}(\mathbf{c}_{12} \cdot \mathbf{t} + R(\omega_1 + \omega_2)\mathbf{t}) \tag{A.65}$$

Solution of the "slip" system (equations (A.57), (A.58), (A.59), (A.60) and (A.61)) is given by

$$\mathbf{c}_1^* - \mathbf{c}_1 = -\frac{1+\epsilon}{2}(\mathbf{c}_{12} \cdot \mathbf{k})(\mathbf{k} + \mu\Lambda\mathbf{t}) \tag{A.66}$$

The rest of post-collisional quantities are obtained directly from (A.57), (A.58), and (A.59) for both "no-slip" and "slip" systems.

The limit between "no-slip" and "slip" conditions can be found by equating (A.65) and (A.66). It is found to be given by condition

$$\tan\gamma_1 = \frac{c_s}{c_n} = \frac{3\mu(1+\epsilon)}{1+\beta} \tag{A.67}$$

where

$$c_n = (\mathbf{g}_{12} \cdot \mathbf{k}); \qquad c_s = (\mathbf{g}_{12} \cdot \mathbf{t}) \tag{A.68}$$

Therefore, for "slip" condition β can be expressed as

$$\beta = -1 + \frac{3\mu(1+\epsilon)}{\tan\gamma} \tag{A.69}$$

For "no-slip" condition, rigid models assume $\beta = \beta_o = \text{const.}$.

In the present model, angular restitution coefficient β is more complex function of parameters μ, ϵ, ζ_s, k_s/k_n as well as of impact angle γ. Coefficient β as calculated by present contact model is plotted in figures A.8 and A.9. It can be observed from these figures that for larger impact angles, corresponding to the cases when the tangential force is at the friction limit during the entire contact ("glancing" collisions), β is proportional to factor $3\mu(1+\epsilon)/\tan\gamma$, exactly as in rigid-particle models. However, for intermediate impact angles, for which one portion of the contact duration is controlled by tangential stiffness and damping, and another portion by friction, the behavior is quite different from simple $\beta = \beta_o$ assumption of rigid models. Finally, for small impact angles, for which the contact is mostly controlled by tangential stiffness and damping, (nearly "head-on" collisions), β asymptotically approaches constant value which is a function of ζ_s and k_s/k_n.

The dependence of β on the ratio k_s/k_n is illustrated in figures A.8.a,b. It can be seen from these figures that β increases over whole range of impact angles as k_s/k_n decreases. The spin reversal phenomenon can be observed for values of k_s/k_n lower than approximately 0.8 at $\zeta_s = 0$. The dependence of β on shear damping coefficient ζ_s is illustrated in figures A.9.a,b. It can be seen from Figure A.9.a. that β is lower for higher values of ζ_s for intermediate impact angles. However, from Figure A.9.b. it can be seen that the effect is opposite for small impact angles, where β is higher for higher ζ_s.

Finally, it is interesting to observe that the β curves obtained by present model are very much similar to β curves obtained by Walton and Braun (1985) using their incrementally slipping frictional model for tangential force.

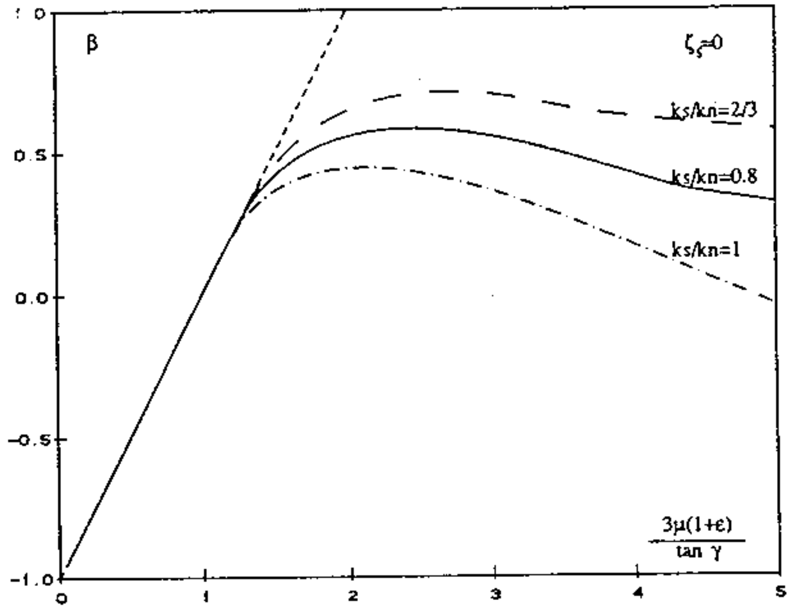

Figure A.8.a. Effect of ks/kn ratio on angular restitution coefficient

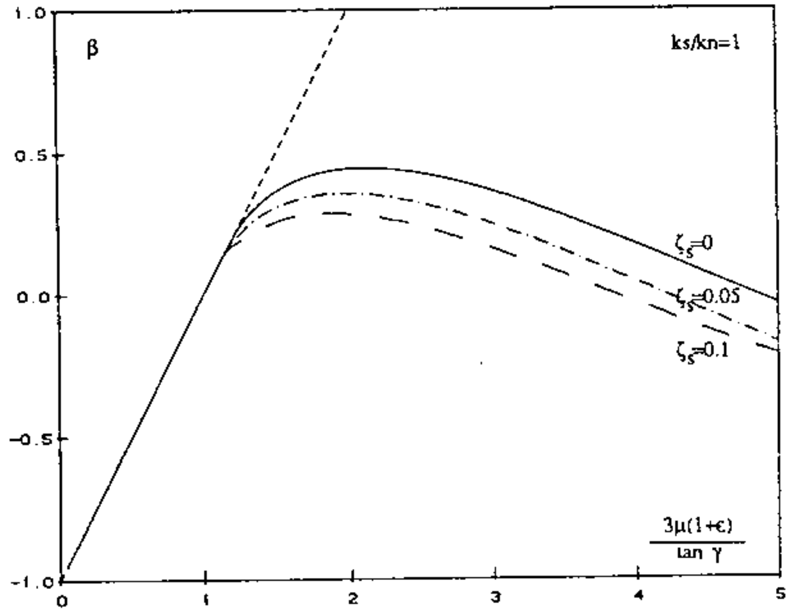

Figure A.9.a. Effect of shear damping on angular restitution coefficient

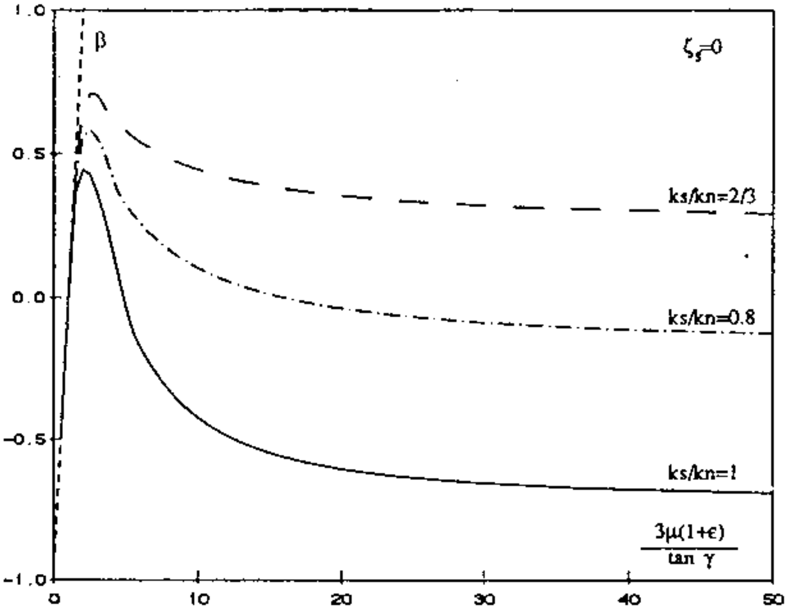

Figure A.8.b. Effect of ks/kn ratio on angular restitution coefficient

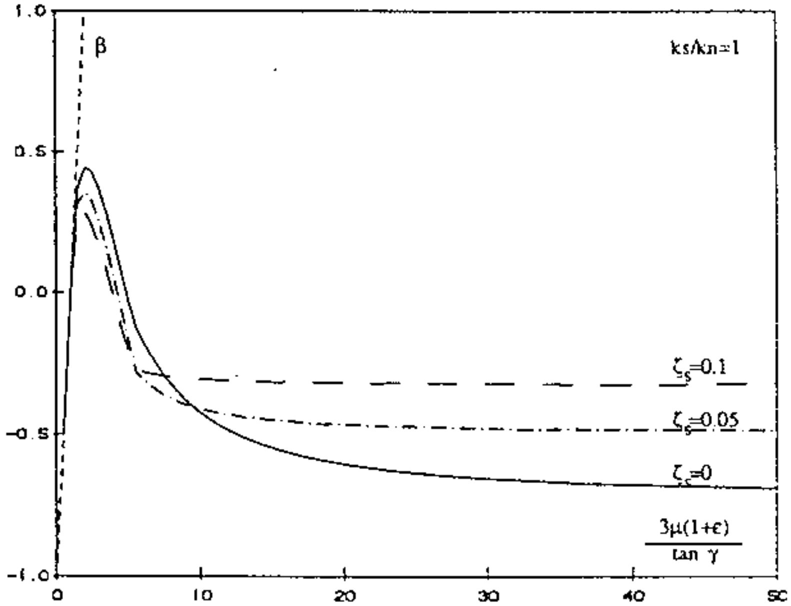

Figure A.9.b. Effect of shear damping on angular restitution coefficient